© 2021. Published by The Company of Biologists Ltd | Development (2021) 148, dev199790. doi:10.1242/dev.199790

RESEARCH ARTICLE

Agrin/Lrp4 signal constrains MuSK-dependent neuromuscular synapse development in appendicular muscle

Lauren J. Walker, Rebecca A. Roque, Maria F. Navarro and Michael Granato*

ABSTRACT

The receptor tyrosine kinase MuSK, its co-receptor Lrp4 and the Agrin ligand constitute a signaling pathway that is crucial in axial muscle for neuromuscular synapse development, yet whether this pathway functions similarly in appendicular muscle is unclear. Here, using the larval zebrafish pectoral fin, equivalent to tetrapod forelimbs, we show that, similar to axial muscle, developing appendicular muscles form aneural acetylcholine receptor (AChR) clusters prior to innervation. As motor axons arrive, neural AChR clusters form, eventually leading to functional synapses in a MuSK-dependent manner. We find that loss of Agrin or Lrp4 function, which abolishes synaptic AChR clusters in axial muscle, results in enlarged presynaptic nerve regions and progressively expanding appendicular AChR clusters, mimicking the consequences of motoneuron ablation. Moreover, *musk* depletion in *lrp4* mutants partially restores synaptic AChR patterning. Combined, our results provide compelling evidence that, in addition to the canonical pathway in which Agrin/Lrp4 stimulates MuSK activity, Agrin/Lrp4 signaling in appendicular muscle constrains MuSK-dependent neuromuscular synapse organization. Thus, we reveal a previously unappreciated role for Agrin/Lrp4 signaling, thereby highlighting distinct differences between axial and appendicular synapse development.

KEY WORDS: Zebrafish, Appendicular, Neuromuscular junction, Agrin, Lrp4, MuSK

INTRODUCTION

Movement depends on the coordinated development of neuromuscular junctions (NMJs) between motor axons and skeletal muscle. Prior to axon arrival, the central region of muscles is 'prepatterned' with clustered acetylcholine receptors (AChR), which requires the receptor tyrosine kinase MuSK. Subsequently, as motor axons contact the muscle and differentiate, they release the glycoprotein Agrin, which binds to the low-density lipoprotein receptor-related protein 4 (Lrp4) on the muscle membrane to stimulate phosphorylation of MuSK. Upon activation, MuSK initiates a downstream signaling cascade to cluster AChRs in apposition to axons, thereby forming neural synapses. Mutants of *lrp4*, *agrn* and *musk* all fail to form NMJs in the mouse and zebrafish trunk, demonstrating their crucial and conserved role in this process (Kim and Burden, 2008; Kim et al., 2008; Zhang et al., 2008; Jing et al., 2010; Remédio et al., 2016; Gribble et al., 2018). Prior work on the Agrin/Lrp4/MuSK pathway in NMJ development has focused predominantly on trunk muscles. In contrast, significantly less is known about the mechanisms crucial for NMJ development in appendicular muscles, which move appendages, such as limbs.

Here, we used the larval zebrafish pectoral fin, analogous to tetrapod forelimbs (Mercader, 2007), to study neuromuscular synapse development in a paired appendage. At 120 h post fertilization [hpf; 5 days post fertilization (dpf)], pectoral fins comprise two antagonistic muscles, the abductor and adductor, separated by an endoskeletal disk (Fig. 1A,B). Each muscle consists of ∼50 fast-twitch (fast) muscle fibers that extend longitudinally from the proximal fin base where it attaches to the trunk, out towards the distal tip of the fin. At the fin base, the abductor and adductor muscles are each two-to-three fibers thick, and thin out to be a single fiber layer throughout most of the fin (Thorsen et al., 2004). The abductor and adductor muscles are innervated by four distinct motor nerves, which we refer to here as nerves 1-4, with cell bodies in anterior spinal cord segments 3-6 (Myers, 1985; Thorsen and Hale, 2007). Motor axons enter the fin at a dorsal (nerves 1-3) or ventral (nerve 4) plexus to sort between the abductor or adductor muscles (Thorsen and Hale, 2007). Axons then progressively defasciculate as they grow towards the distal tip of the fin, such that each muscle fiber is polyinnervated and motor axons create a patchwork pattern across the fin muscles. This innervation pattern remains unchanged until juvenile stages at 3 weeks post-fertilization (5.4-5.8 mm) when the muscles divide, nerves arborize and bone forms (Grandel and Schulte-Merker, 1998; Thorsen and Hale, 2007). The genetic tractability, availability of transgenic tools to label specific cell types, optical transparency suitable for live imaging, and behavioral readout of fin movement make the larval zebrafish pectoral fin an ideal vertebrate system to interrogate mechanisms of neuromuscular synapse development within appendicular muscles.

The axial trunk and pectoral fin neuromuscular systems differ in several key ways. First, axon innervation of trunk muscles begins between 16 and 24 hpf (Eisen et al., 1986), whereas, in appendicular/fin muscles, it starts approximately 24 h later. Second, the trunk comprises several medial layers of fast muscle fibers and a single lateral slow-twitch (slow) muscle fiber layer, which are arranged in repeating segments. In contrast, the fin muscles are only one fiber thick, comprise solely fast fibers (Patterson et al., 2008; Thorsen and Hale, 2007) and are ∼2.5 times longer than trunk muscle fibers. Additionally, after exiting the spinal cord, axons in the trunk grow perpendicular to, and along the center of, muscle fibers. In contrast, motor axons that innervate the pectoral fin grow through the body wall, sort at a plexus and then branch to create elaborate innervation patterns across fin muscle fibers. Axonal innervation of the fin is topographic, with axons from anterior spinal segments innervating the dorsal fin and axons from posterior segments innervating the ventral fin

Department of Cell and Developmental Biology, Perelman School of Medicine, University of Pennsylvania, Philadelphia, PA 19104, USA.

*Author for correspondence (granatom@pennmedicine.upenn.edu)

L.J.W., 0000-0003-3844-4275; R.A.R., 0000-0002-5850-3212; M.G., 0000-0003-3878-9468

Handling Editor: Steve Wilson
Received 12 May 2021; Accepted 24 September 2021

Development (2021) 148, dev199790. doi:10.1242/dev.199790

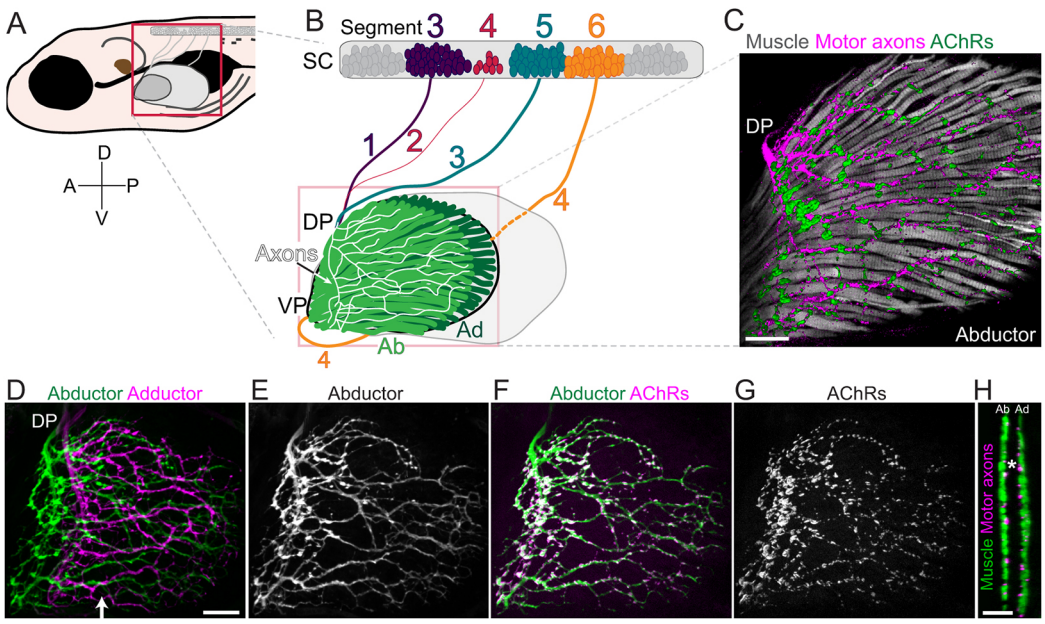

Fig. 1. Pectoral fin anatomy. (A) Schematic of a 120 hpf (5 dpf) zebrafish larva. The boxed area indicates the region shown in more detail in B. (B) Schematic of pectoral fin motoneuron innervation. Motoneuron cell bodies are in spinal cord (SC) segments 3-6. Nerves 1-3 enter the fin at the dorsal plexus (DP), whereas nerve 4 (orange line) enters the fin at the ventral plexus (VP). All nerves innervate both the abductor (Ab) and adductor (Ad) muscles. (C) Ab innervation of a 120 hpf *Tg(α-actin:GFP);Tg(Xla.Tubb:DsRed)* pectoral fin stained with α-Btx to visualize muscle fibers, axons and AChRs (*n*=7 larvae). (D) Maximum projection of *Tg(mnx1:GFP)* innervation in the pectoral fin. Ab (green) and Ad (magenta) innervation patterns are pseudo-colored. (E) Ab innervation alone. (F) Ab innervation showing AChRs. (G) AChR labeling alone. *n*>77 WT pectoral fin images for D-G. (H) Cross-section of pectoral fin at approximate region marked by arrow in D. Asterisk marks the endoskeletal disk that separates the two muscles. A, anterior; D, dorsal; P, posterior; V, ventral. Scale bars: 25 µm.

(Thorsen and Hale, 2007). Finally, in the trunk, aneural AChRs are present on slow muscle fibers, which are absent in the pectoral fin (Flanagan-Steet et al., 2005). Whether AChRs are prepatterned and how axon outgrowth occurs in the pectoral fin have not yet been described.

Although many of the signals that mediate NMJ development have been well characterized in trunk muscles, whether the same cellular and molecular mechanisms underlie NMJ development within the complicated muscle arrangement of paired appendages has remained unclear. Here, we reveal that, although some aspects of neuromuscular synapse development, such as prepatterning with aneural AChR clusters and the requirement for MuSK to form AChR clusters, are shared between the trunk and the pectoral fin, there are key muscle-specific differences. We show that both axonally released Agrin and Lrp4 on muscle cells are required to form the distributed patterning of AChR clusters in the fin. Whereas *agrn* and *lrp4* mutants fail to form synapses in the trunk, in the pectoral fin they instead form giant AChR clusters and axonal innervation abnormalities. A developmental time course in *agrn* mutant fins reveals that these clusters likely arise from prepatterned AChR clusters that grow over time. These giant clusters sequester navigating growth cones, thereby disrupting the innervation patterning. Partial depletion of *musk* moderately suppresses the formation of these clusters in *agrn* and *lrp4* mutants. Based on our results, we propose a model for NMJ formation in the appendicular fin muscle in which Agrin/Lrp4 signaling transitions MuSK from a prepatterning state to an axon-dependent, focal AChR-clustering state. Without Agrin or Lrp4, MuSK-dependent signaling remains active within prepatterned islands and AChR clusters grow. Importantly, this work exposes key differences in neuromuscular synapse development between axial muscles of the trunk and appendicular muscles of the pectoral fin.

RESULTS

Development of pectoral fin innervation is a tightly coordinated and dynamic process

At 120 hpf, zebrafish pectoral fin motor axons have an elaborate pattern across the abductor and adductor muscles. To compare the organization between nerve and muscle within the fin, we used transgenic *mnx1*:*GFP* or *Xla.tubb*:dsRed to visualize most, if not all, motor axons innervating the pectoral fin, and *α-actin:GFP* to label pectoral fin muscle fibers (Fig. 1A-C). Although the fin comprises both abductor and adductor muscles with independent innervation fields (Fig. 1D,H), for simplicity we include only abductor innervation unless otherwise noted (Fig. 1E-G). Labeling of nicotinic AChRs with α-bungarotoxin (α-Btx) revealed hundreds of small, evenly spaced, *en passant* neuromuscular synapses juxtaposed to motor axons (Fig. 1F,G). The largest postsynaptic AChR clusters were associated with the major nerve branch closest to the proximal fin base, whereas AChR clusters became smaller as the finer nerve branches defasciculated towards the distal fin tip.

Previous work has described the development of the fin (Yano et al., 2012; Siomava et al., 2018), as well as the innervation and musculature of the fin after 120 hpf (Thorsen and Hale, 2007), a time point at which the larval innervation pattern is relatively stable. To our knowledge, the development of the zebrafish pectoral fin musculature and its complex innervation pattern prior to 120 hpf have not been described. To observe this process dynamically, we used time-lapse imaging of transgenic embryos to observe muscles [*Tg(α-actin:GFP)*] and axons [*Tg(Xla.tubb*:dsRed*)*]. By approximately prim-25 (36 hpf), motor axons from nerves 1-3 coalesced at the future dorsal plexus, and nascent muscle fibers in the pectoral fin bud, located laterally to the axons, had just started expressing *α-actin*:*GFP* (Fig. 2A,B; Movie 1). Muscle fibers continued to reorganize through the long-pec stage as the fin moved

Development (2021) 148, dev199790. doi:10.1242/dev.199790

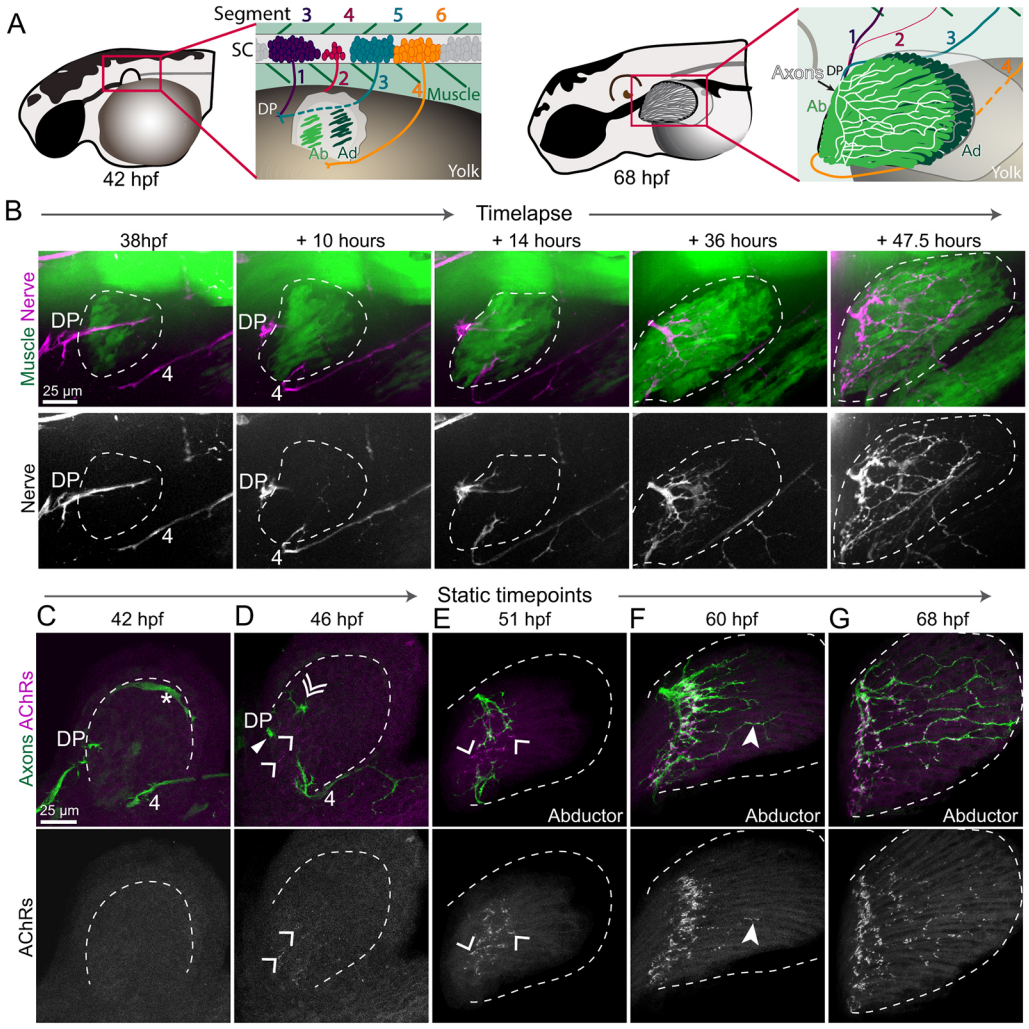

Fig. 2. Development of pectoral fin innervation. (A) Schematic of zebrafish larvae at 42 hpf (high-pec stage) and 68 hpf (pec fin stage). The boxed regions indicate the areas highlighted in the insets, showing motoneurons from spinal cord (SC) segments 3-6 and their corresponding nerves (1-4) projecting to the dorsal plexus (DP) to innervate the abductor (Ab) and adductor (Ad) muscles of the pectoral fin. (B) Maximum projection stills from time-lapse imaging of *Tg(α-actin:GFP);Tg(Xla.Tubb:DsRed)* larvae showing muscles and axons. Dashed lines outline pectoral fin musculature. Axons converge at the DP prior to innervating nascent muscle fibers. As muscle fibers elongate, the axonal innervation pattern elaborates (*n*=7 WT fins). Static time points of *Tg(mnx1:GFP)* larvae stained with α-Btx to label AChRs. Nerve 4 is indicated by '4'. (C) At 42 hpf, the pectoral fin bud is still lateral to the DP; thus, axons and muscles are not yet in the same plane. Asterisk indicates vasculature also labeled by *mnx1:GFP*. (D) Axons have just grown past the DP. Ab axons are indicated by the filled triangle, Ad axons are indicated by the double arrowhead and aneural AChR clusters are indicated by single arrowheads. (E-G) Ab innervation only. Axons occupy prepatterned clusters and induce new AChR clusters as they grow throughout the fin. Filled arrowhead indicates a fin axon branch already associated with AChR clusters. Single arrowheads indicate aneural AChR clusters. *n*=5-10 pectoral fins per time point for C-G.

further medially, closer to the plane of the dorsal plexus; motor axons began to grow into the abductor and then adductor muscles beginning around the long-pec stage at 46 hpf. Concurrently, axons in nerve 4 made a sharp turn dorsally to innervate the fin via the ventral plexus. Thick axon bundles first grew perpendicular to muscle fibers near the proximal fin base and, subsequently, axons turned posteriorly to grow mostly parallel to muscle fibers and towards the fin tip. As muscle fibers elongated, branching motor axons followed close behind, forming a diffuse innervation network. By ∼68 hpf, a simplified innervation pattern was recognizable (Fig. 2B,G) that became more complex through 120 hpf. Thus, pectoral fin neuromuscular development is a highly dynamic yet tightly coordinated process.

Pectoral fins start moving rhythmically around 72 hpf (Uemura et al., 2020), prompting us to examine when neuromuscular synapses form in the pectoral fin. To observe neuromuscular synapse development in pectoral fins, we fixed transgenic *mnx1:GFP* larvae (to label presynaptic motor axons) at various time points and labeled AChRs with α-Btx. In vertebrates, 'prepatterned' AChR clusters form on muscle fibers prior to motoneuron innervation (Lin et al., 2001; Yang et al., 2001), but whether or when this occurs in appendicular muscle of pectoral fins is unclear. At the high-pec stage (∼42 hpf), when the pectoral fin bud is located lateral to the nascent dorsal plexus and axons have not yet entered the fin, AChR clusters were undetectable (Fig. 2C). By 46 hpf, as axons had just started to grow past the plexus onto the fin musculature, we observed small AChR clusters near the base of the fin that were not yet associated with labeled axons (Fig. 2D). At 51 hpf, axons growing from the dorsal and ventral plexi extended towards each other along the fin base and innervated nearby AChR clusters, whereas remaining aneural AChR clusters at the not-yet-innervated medial region of the fin increased in size (Fig. 2E). By 60 hpf, all

Development (2021) 148, dev199790. doi:10.1242/dev.199790

AChR clusters at the proximal fin base were associated with axons (Fig. 2F).

The entry of axons into the fin initiated a second phase of neuromuscular synapse formation. As axons grew beyond the fin base and branch to extend along muscle fibers, new AChR clusters emerged. These new AChR clusters were always associated with axons (Fig. 2F,G). The number of AChR clusters increased as the innervation pattern became more complex and, by 120 hpf, axons were associated with hundreds of regularly spaced AChR clusters that remained relatively small (<5 µm^2) (Fig. 2G). In contrast, clusters at the fin base that preceded axon outgrowth continued to increase in size, such that, by 120 hpf, the biggest AChR clusters in the fin (>20 µm^2) were in this proximal region. Thus, neuromuscular synapse development in appendicular muscle of the pectoral fin mirrors that in axial muscle of the trunk, with a prepatterned phase and an axon-associated phase of synapse formation.

MuSK signaling is required for neuromuscular synapse development in pectoral fin muscle

Given the similarities in AChR prepatterning and axon-associated AChR clustering, we investigated whether the well-established genetic pathway that regulates neuromuscular synapse development in axial muscle is also required for this process in pectoral fin muscle. In vertebrate axial muscles, AChR prepatterning and the formation of neuromuscular synapses requires the receptor tyrosine kinase MuSK (DeChiara et al., 1996; Lefebvre et al., 2007). By staining sibling and *musk* mutant pectoral fins with α-Btx to label AChR clusters, we first determined whether *musk* is also required for AChR prepatterning within larval zebrafish appendicular muscle. At the long-pec stage (46 hpf), when wild-type (WT) sibling animals had developed robust prepatterned aneural AChR clusters, staining of *musk*-mutant pectoral fins failed to reveal any prepatterned AChR clusters (Fig. S1). To account for a delay in pectoral fin development or aneural cluster formation, we also examined *musk* mutants at later time points. At 51 hpf and 60 hpf, the extent of axon growth in the fin was comparable between siblings and *musk* mutants. At these time points, WT axons had innervated prepatterned AChR clusters and new clusters had formed, whereas in *musk* mutant fins α-Btx staining remained diffuse and muscles lacked discernible AChR clusters. Thus, as in trunk axial muscle, *musk* is required for AChR prepatterning in appendicular fin muscle.

Next, we examined the role of MuSK in the formation of neural AChR clusters characteristic of neuromuscular synapses. In the zebrafish trunk, motor axons branch and form synapses distributed along myofibers throughout the myotome. Consistent with previous work (Lefebvre et al., 2007; Jing et al., 2010), at 120 hpf, compared with sibling controls, trunk axial muscle fibers in *musk* mutants exhibited diffuse α-Btx staining with fewer and smaller AChR clusters (Fig. 3A,B,D). Similar to trunk axial muscle fibers, appendicular muscle fibers in *musk* mutants displayed mostly

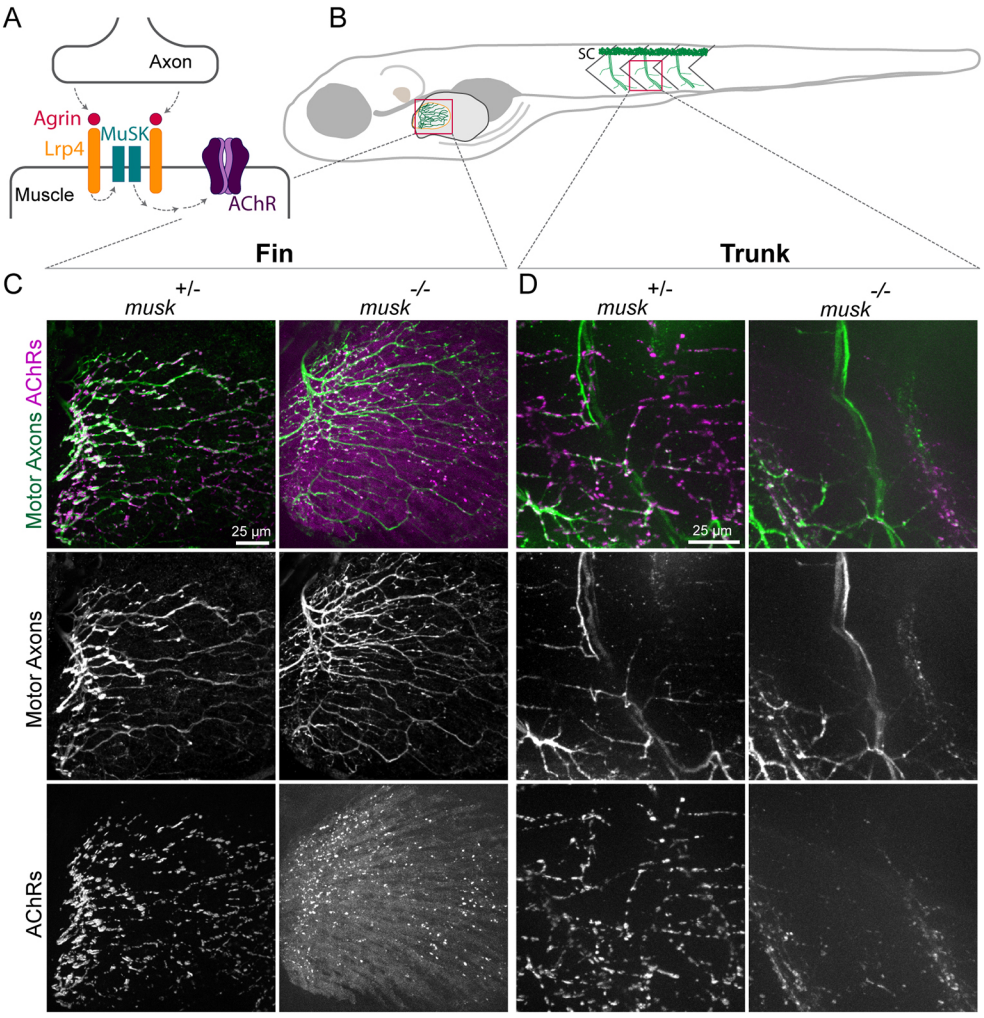

Fig. 3. MuSK is required for pectoral fin neuromuscular synapse development. (A) Schematic of the Agrin/Lrp4/MuSK pathway. (B) Schematic of a larval zebrafish at 120 hpf. Red boxes outline regions of the fin and trunk that are shown in C,D. (C) Abductor muscle innervation in the pectoral fin in 120 hpf larvae expressing *Tg(mnx1:GFP)* to label motoneurons and stained with α-Btx to label AChRs. *musk* heterozygous sibling pectoral fins exhibit an innervation pattern with numerous small AChR clusters (*n*=45/45), whereas *musk* mutants have an exuberant innervation pattern with diffuse AChR signal throughout muscle fibers in the fin and some focal AChR clusters (*n*=25/25). (D) Trunk innervation from the same animals shown in C. *musk* mutants form fewer and smaller neuromuscular synapses compared with sibling controls. SC, spinal cord.

Development (2021) 148, dev199790. doi:10.1242/dev.199790

diffuse α-Btx staining and lacked WT-like AChR clusters (Fig. 3C). Whereas *musk* mutants exhibited some AChR clusters that form in apposition to axons, they were fewer and smaller in size compared with sibling controls. These circular clusters resembled the dystroglycan-dependent clusters that form on zebrafish axial muscle fibers in the absence of *musk* (Lefebvre et al., 2007). Moreover, compared with WT controls, motor axons in *musk* mutant pectoral fins were less fasciculated, similar to that reported previously for trunk muscle fibers in zebrafish and mice lacking MuSK (Kim and Burden, 2008; Jing et al., 2009).

Finally, we asked whether MuSK acts through its well-established downstream effector Rapsyn during appendicular neuromuscular development. Like *musk*, *rapsyn* is required for AChR clustering in mouse and zebrafish axial muscle (Gillespie et al., 1996; Ono et al., 2002). Similar to its role in axial muscle, *rapsyn* is required for AChR clustering in the pectoral fin, as *rapsyn* mutants displayed diffuse α-Btx signal throughout pectoral fin muscles (Fig. S2). In contrast to *musk* mutants, in which pectoral fin axons were defasciculated and overgrown (Figs 3C and 7B), motoneuron innervation in the pectoral fin of *rapsyn* mutants was indistinguishable from that of WT (Fig. S2), similar to observations of *rapsyn*-mutant trunk innervation (Zhang et al., 2004; Gribble et al., 2018). Thus, *musk* and *rapsyn* are required for NMJ development in the pectoral fin, suggesting that postsynaptic mechanisms crucial for synapse formation are shared between trunk and appendicular muscle.

Axonal derived signals are crucial for appendicular AChR patterning

NMJ development requires bidirectional coordination between axons and muscles. To determine the effect of motor axon-derived signals on the postsynaptic innervation pattern, we laser-ablated the motoneurons innervating the dorsal portion of the pectoral fin muscle. Specifically, we ablated the cell bodies of motoneurons in spinal segments 3-5 at 42 hpf, prior to the growth of motor axons into the pectoral fin bud, and then re-ablated any newly formed motoneurons 24 h later. Importantly, we left intact all motoneurons in spinal segment 6, which innervate the ventral muscle region of the fin, to serve as an internal control when comparing the innervation patterns of innervated and nerve-deprived muscle fibers. At 120 hpf, AChR patterning in the innervated ventral region of the fin was indistinguishable compared with non-ablated controls, with small, evenly spaced AChR clusters apposed to axons (Fig. 4A-C). Surprisingly, in the dorsal region of motoneuron-ablated fins that had never been innervated, fewer but much larger AChR clusters formed (Fig. 4C). These clusters were globular and evenly dispersed throughout the non-innervated musculature and differed vastly in size and distribution from those observed in the absence of MuSK or Rapsyn (Fig. 3; Fig. S2). Formation of these abnormal clusters requires MuSK, as motoneuron-ablated *musk*-mutant pectoral fins exhibited diffuse α-Btx staining similar to innervated *musk*-mutant fins (Fig. S3). Thus, whereas lack of the postsynaptic signal transduction machinery blocks the formation of AChR clusters almost completely, the absence of axonal-derived signals results in unpatterned yet exuberantly sized AChR clusters, which we refer to as giant AChR clusters. We conclude that axonal-derived signals are crucial for AChR patterning and for limiting AChR cluster size.

Agrin and Lrp4 are required for appendicular neuromuscular development

The opposing consequences of blocking MuSK-dependent postsynaptic signaling versus eliminating all presynaptic signaling prompted us to examine the role of signaling components that activate MuSK. Axon-derived Agrin coordinates MuSK-dependent AChR clustering between nerve terminals and muscle fibers (Kim et al., 2008; Zhang et al., 2008), and zebrafish mutants lacking the motoneuron-derived Agrin isoforms lack synaptic AChR clusters along axial trunk muscle fibers (Fig. 5A) (Gribble et al., 2018).

Therefore, we hypothesized that Agrin has a similar crucial role in inducing neural AChRs in pectoral fin muscle. Throughout the fin of siblings, hundreds of <5 μm^2 AChR clusters were evenly distributed along muscle fibers. In contrast, AChR clusters in *agrn* mutants were reduced in number but increased in size (>20 μm^2) (Fig. 5B,E), indistinguishable from the giant AChR clusters in nerve-deprived fins (Fig. 4C). To quantify the number of neural AChR clusters and their size distribution across genotypes, we focused on abductor muscle fibers, although quantification of adductor muscles across all genotypes revealed similar results (Fig. S4). Sibling abductor muscle fibers exhibited 294.4±21.5 α-Btx-positive AChR clusters per fin with a median cluster size of 3.9±0.6 μm^2 (Fig. 5C-E). In contrast, *agrn*-mutant abductor muscle fibers had significantly fewer clusters per fin (51.6±5.9, unpaired *t*-test P<0.0001) but exhibited a vastly increased median cluster size of 18.4±4.7 (unpaired *t*-test P<0.0001). Thus, in striking contrast to *agrn*-mutant trunk muscle fibers, which exhibited smaller AChR clusters

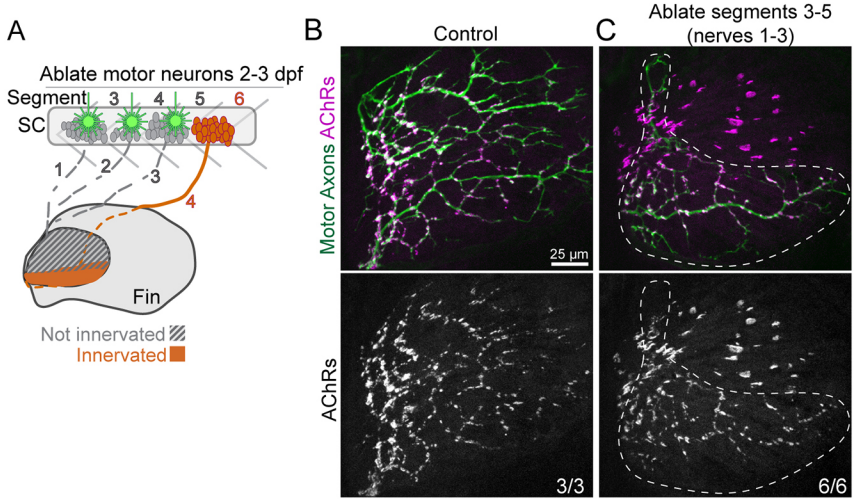

Fig. 4. Pectoral fin muscles are predisposed to form large AChR clusters. (A) Motoneuron cell bodies from spinal cord (SC) segments 3-5 were laser ablated at 2 and 3 dpf to prevent motor axon innervation of the dorsal pectoral fin. (B) Pectoral fins from control *Tg(mnx1:GFP)* larvae stained with α-Btx to label AChRs. (C) Pectoral fins from *Tg(mnx1:GFP)* WT larvae after motoneuron ablation at 120 hpf (5 dpf). The ventral fin is innervated (white-dashed region) with input from unablated nerve 4 (segment 6). The non-innervated dorsal region of the fin has enlarged AChR clusters.

Development (2021) 148, dev199790. doi:10.1242/dev.199790

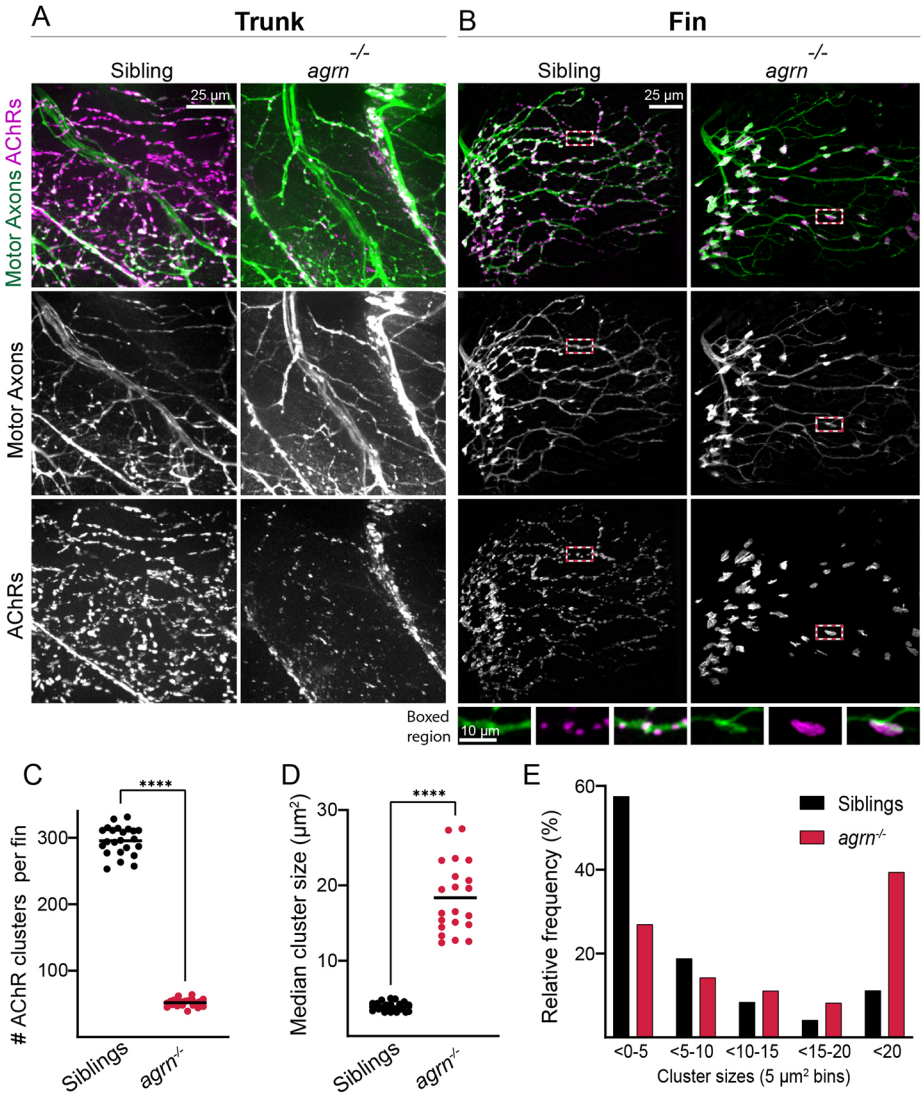

Fig. 5. Agrin is required for correct axon innervation and AChR patterning in the pectoral fin. (A) Trunk innervation in 120 hpf larvae expressing *Tg(mnx1:GFP)* to label motor axons and stained with α-Btx to label AChRs. Trunks in *agrn* mutants form fewer and smaller neuromuscular synapses. (B) Abductor muscle innervation in the pectoral fin from the same animals shown in A. *Agrn* siblings exhibit an innervation pattern with numerous small AChR clusters, whereas *agrn* mutants have swellings in the innervation pattern directly opposed to enlarged AChR clusters throughout muscle fibers in the fin. Insets from boxed regions show an even distribution of small AChR clusters (magenta) in siblings, whereas mutants have large AChR clusters that colocalize with green axon swellings. All images are maximum intensity projections that include the same number of slices for each genotype. (C,D) Quantification of the number of AChR clusters per fin (C) and the median cluster size per fin (D). (E) Histogram of the distribution of AChR cluster sizes across all fins quantified (5 µm^2 bins). ****P<0.0001, unpaired t-test. n=23 (siblings), 21 (mutants).

[median cluster size, siblings: 3.5±0.7 µm^2 (n=17), *agrn*$^{-/-}$: 1.7±0.7 µm^2 (n=9), unpaired t-test P<0.0001], *agrn*-mutant appendicular muscle fibers exhibited greatly enlarged AChR clusters.

The strikingly divergent appendicular NMJ phenotypes observed in *musk* mutants characterized by an almost-complete loss of AChR clusters versus the giant AChR clusters present in *agrn* mutants prompted us to examine the role of the Agrin receptor Lrp4. Upon binding Agrin, Lrp4 induces MuSK phosphorylation to initiate synaptic differentiation (Kim et al., 2008; Zong et al., 2012). To determine whether *lrp4* mutants display the phenotype exhibited by its ligand Agrin or by its co-receptor MuSK, we examined the role of Lrp4 in appendicular neuromuscular development. Similar to *musk* and *agrn*, *lrp4* is required for NMJ development in axial muscles of the zebrafish trunk, because mutants form fewer and smaller synapses (Remédio et al., 2016). Identical to the *agrin*-mutant fin phenotype and in contrast to the *lrp4*-mutant phenotype in axial trunk muscles, at 120 hpf, *lrp4*-mutant pectoral fin muscles displayed large AChR clusters (Fig. 6A,B,D-F). Moreover, in fins of *lrp4* mutants lacking the intracellular domain (Saint-Amant et al., 2008), we also observed giant AChR clusters (Fig. S5), providing compelling evidence that Lrp4 acts through a ligand-dependent mechanism to regulate appendicular NMJ development. Importantly, the overall number and morphology of *Tg(α-actin:GFP)*-positive pectoral fin muscle fibers in *lrp4* mutants were indistinguishable from that observed in siblings, indicating that appendicular muscle development is unaffected in *lrp4* mutants (Fig. S5). Finally, expressing Lrp4 using a muscle-specific promoter *Tg(α-actin:lrp4-GFP)* (Gribble et al., 2018) in otherwise *lrp4*-mutant animals fully restored appendicular synapse development (Fig. 6C-F), indicating that Lrp4 functions in muscle. Thus, loss of Agrin or Lrp4, although associated with a significant reduction in neural AChR cluster numbers in both axial and appendicular muscle, leads to an increase in AChR cluster size on appendicular muscle, distinct from their mutant phenotypes in axial muscle.

Agrin/Lrp4 regulates the size and patterning of appendicular neuromuscular synapses

The giant AChR clusters we observed on *agrn*- and *lrp4*-mutant appendicular muscles resembled those previously described in *Xenopus* and chick muscle cells grown in the absence of axons as AChR 'hot spots', which disperse upon innervation (Bekoff and Betz, 1976; Moody-Corbett and Cohen, 1982; Peng, 1986). Therefore, we investigated whether the giant AChR clusters we observed in *agrn*- or *lrp4*-mutant pectoral fins are caused by the lack of axonal innervation. Analysis of axonal innervation patterns at

Development (2021) 148, dev199790. doi:10.1242/dev.199790

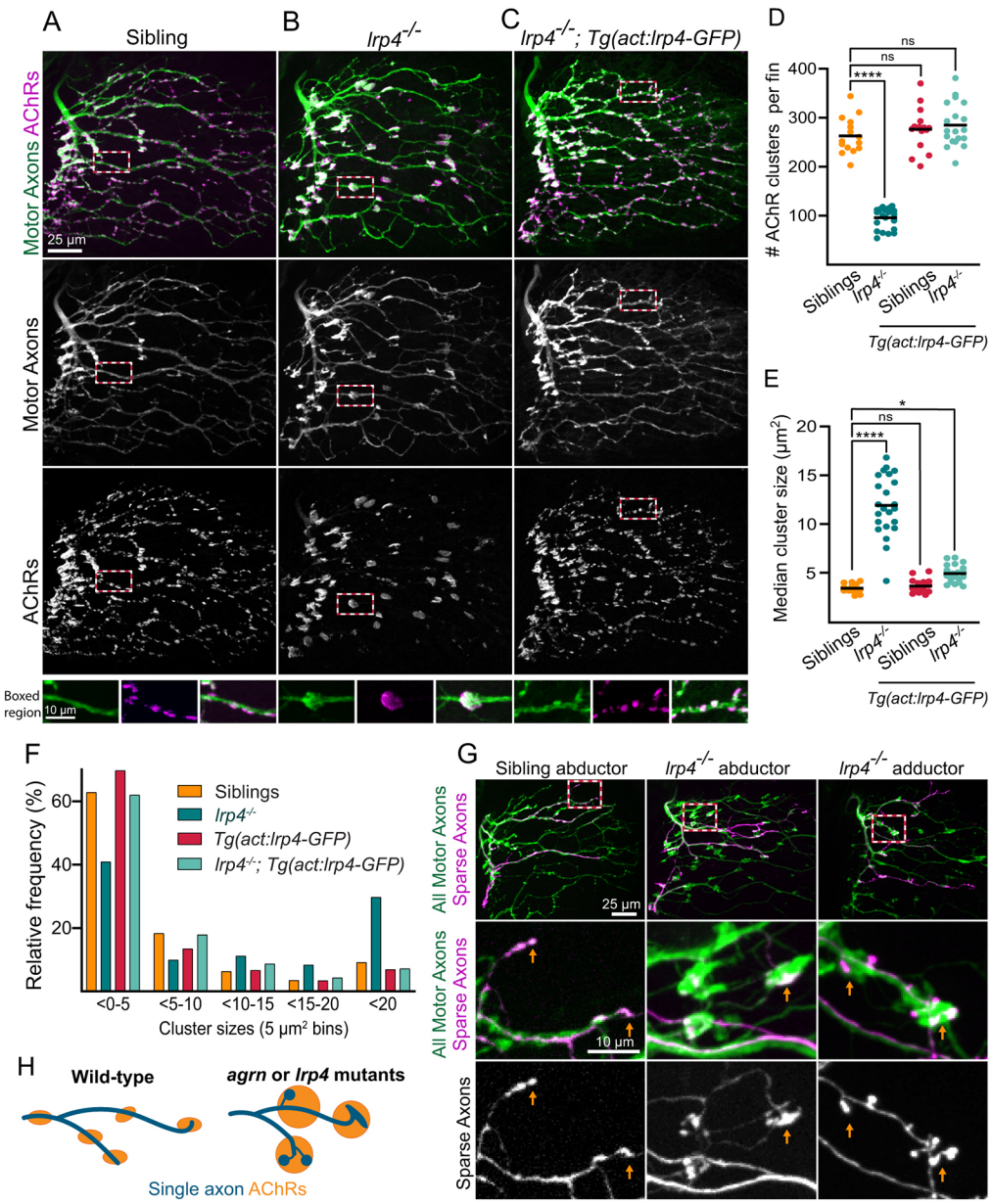

Fig. 6. Lrp4 is required for correct axon innervation and AChR patterning in the pectoral fin. (A-C) Abductor muscle innervation in the pectoral fin in 120 hpf larvae expressing *Tg(mnx1:GFP)* to label motoneurons and stained with α-Btx to label AChRs. (A) *lrp4* siblings exhibit innervation patterns with numerous small AChR clusters. (B) *lrp4* mutants exhibit abnormal swellings in an innervation pattern directly opposed to that of large AChR clusters. (C) Expression of *lrp4-GFP* in muscles of *lrp4* mutants is sufficient to rescue the mutant innervation pattern. Boxes outline the regions shown in insets. (D,E) Quantification of the number of AChR clusters per fin (D) and the median cluster size per fin (E). (F) Histogram of the distribution of AChR cluster sizes across all animals quantified (5 µm^2 bins). *n*=15 (siblings), 23 (*lrp4* mutants), 16 [siblings plus *Tg(act:lrp4-GFP)*], 20 [*lrp4* mutants plus *Tg(act:lrp4-GFP)*]. (G) Sparse labeling of axons injected with *mnx1:mKate*, with all motor axons labeled with *Tg(mnx1:GFP)*. Sparse labeling does not label entire 'swelling' but axon ends appear bulbous, indicating that multiple axons contribute to the abnormal innervation swellings in *lrp4* mutants. Orange arrows indicate axon endings. Boxed indicate the regions magnified below. *n*=11/12 (sibling fins), 7/7 (mutant fins). (H) Schematic summarizing axonal organization and AChR clusters. ns, not significant. **P*<0.05, *****P*<0.0001, one-way ANOVA with Dunnett's multiple comparisons test.

120 hpf revealed that, in both *agrn* and *lrp4* mutants, the overall pectoral fin innervation pattern was comparable to that of WT, indicating that axon guidance mechanisms are largely intact. However, unlike in siblings, in both *agrn*- and *lrp4*-mutant fins, we observed large *mnx1:GFP*-positive innervation 'swellings' (Fig. 5B; Fig. 6B). These swellings colocalized with the enlarged postsynaptic AChR clusters, supporting the notion that, rather than being aneural AChR hot spots, these giant AChR clusters are indeed innervated and do not disperse upon axon contact. Moreover, expressing Lrp4 using the muscle-specific promoter *Tg(α-actin:lrp4-GFP)* (Gribble et al., 2018) in otherwise *lrp4*-mutant animals fully suppressed formation of presynaptic axonal swellings (Fig. 6C-F), indicating that muscle-derived Lrp4 signaling plays a role in establishing both presynaptic and postsynaptic neuromuscular synapse patterning.

To further investigate the nature of these innervation swellings, we used the Znp-1 antibody against the presynaptic marker Synaptotagmin 2. In control pectoral fins, the Znp-1 signal concentrated at α-Btx-positive postsynaptic areas, demarcating presumptive presynaptic sites. Similarly, in *agrn*-mutant pectoral fins, the Znp-1 signal colocalized with the giant AChR clusters (Fig. S6). Furthermore, localization of the postsynaptic protein Dystrophin (Dmd) to synaptic regions was maintained in *lrp4*-mutant pectoral fins (Fig. S7). Thus, whereas in *agrn* and *lrp4* mutants, AChR cluster size and distribution were altered, both presynaptic and postsynaptic proteins were recruited to these giant clusters. Finally, compared with WT siblings, movement was largely unaffected in *lrp4*-mutant pectoral fins (Fig. S8), suggesting that giant AChR clusters represent *bona fide* functional synapses.

We next examined the prominent presynaptic 'swellings' in *lrp4* and *agrn* mutants that form in opposition to enlarged AChR clusters at the single axon level. To do so, we sparsely labeled axons using *mnx1:m*Kate in the context of the entire population of motor axons (*mnx1:GFP*). In siblings, we found that individual axons branched and fasciculated with other axons to form complex patterns. Axons terminated abruptly, with endings approximately the same diameter as the rest of the labeled axon (Fig. 6G,H). In *lrp4* mutants, most individually labeled axons exhibited similarly complex trajectories,

Development (2021) 148, dev199790. doi:10.1242/dev.199790

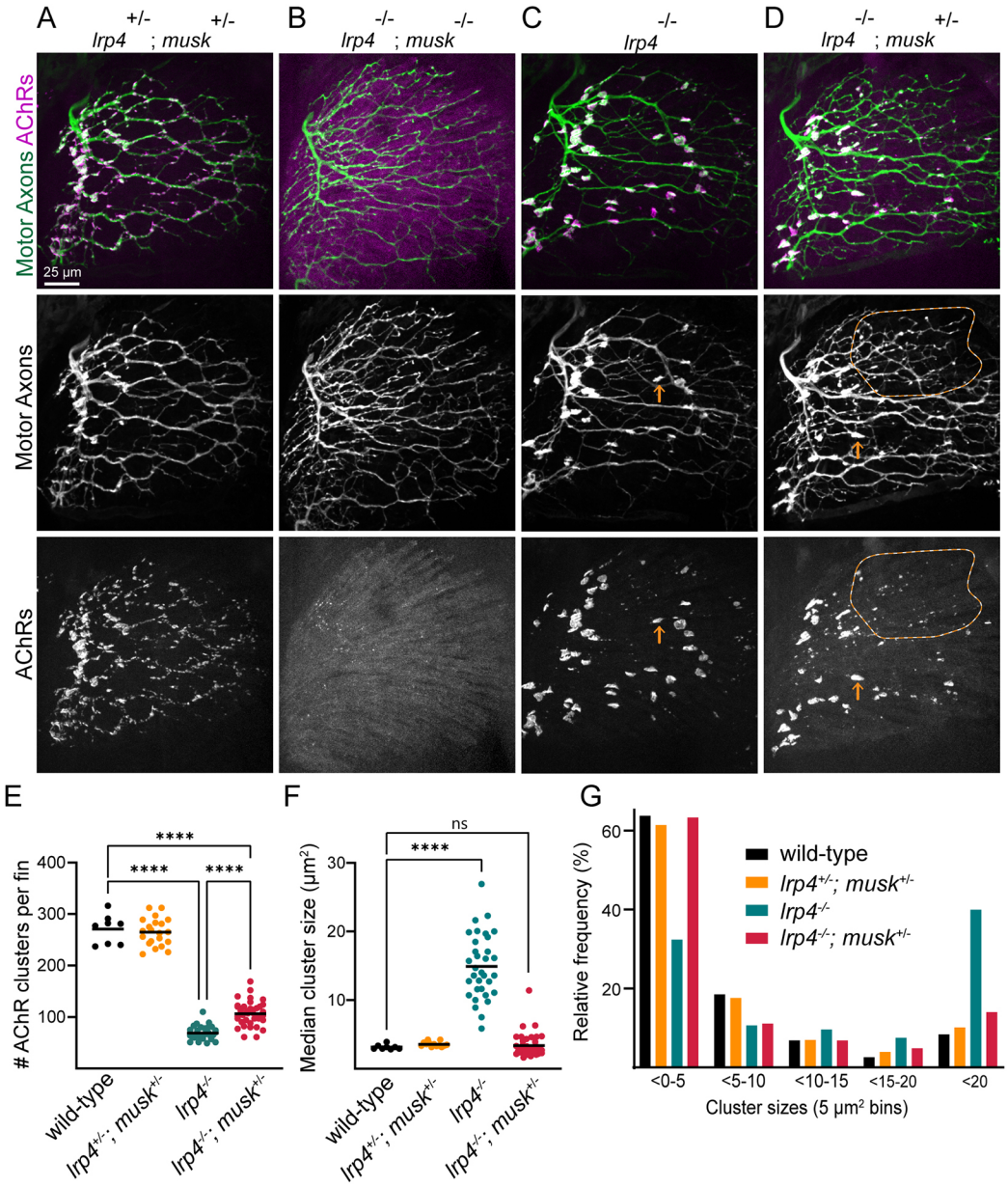

Fig. 7. Musk depletion partially suppresses *lrp4*-mutant phenotype. (A,B) *lrp4*$^{+/-}$;*musk*$^{+/-}$ trans heterozygotes have an innervation pattern indistinguishable from WT (A), whereas *lrp4;musk* double mutants phenocopy *musk* mutants with defasciculated axonal patterning labeled with *Tg(mnx1:GFP)* and diffuse AChR staining labeled by α-Btx (B). (C) *lrp4*-mutant motor axons have swellings in their innervation pattern that are opposed to large AChR clusters. (D) Although *lrp4* mutants that are heterozygous for *musk* (*lrp4*$^{-/-}$;*musk*$^{+/-}$) still have some large AChR clusters similar to *lrp4* mutants (orange arrows), they also have regions of the fin with smaller AChR clusters (encircled by orange line). (E-G) Quantification of the number of AChR clusters per fin (E), the median cluster size per fin (F) and the distribution of cluster sizes (5 µm^2 bins) (G). ****P<0.001, one-way ANOVA with Sidak's (E) or Dunnett's (F) multiple comparisons test. n=8 (WT), 21 (*lrp4*$^{+/-}$;*musk*$^{+/-}$), 4 (*lrp4*$^{-/-}$;*musk*$^{-/-}$), 33 (*lrp4*$^{-/-}$) and 39 (*lrp4*$^{-/-}$;*musk*$^{+/-}$).

were similar in diameter to sibling controls and occasionally formed simplified endings. However, we also observed individual *mnx1:Kate*-positive axons that formed bulbous and swollen structures. These globular endings of *mnx1*:*mKate* axons were part of larger *mnx1:GFP* swellings, indicating that multiple axons contribute to these swellings. These swellings colocalized with α-Btx (Fig. 6B), consistent with the idea that, despite their abnormal morphology, they represent axonal terminals. In further support of this conclusion, electron microscopy revealed that, in *lrp4* mutants, multiple vesicle-positive axonal processes contributed to these enlarged terminals, reminiscent of presynaptic regions (Fig. S9). These results strongly suggest that, during appendicular neuromuscular development, Agrin/Lrp4-dependent signaling not only promotes the formation of postsynaptic AChR clusters, but also limits their size. In addition, Agrin/Lrp4 signaling also influences presynaptic patterning. Thus, our data reveal that the roles of Agrin and Lrp4 in zebrafish appendicular fin are distinctly different from their well-characterized functions in trunk axial muscle.

musk depletion partially suppresses the *lrp4* giant AChR cluster phenotype

Our results reveal that, unlike in trunk muscle of mice and zebrafish, *musk*-mutant appendicular muscle displayed an almost-complete loss of AChR clusters, whereas *agrn*- and *lrp4*-mutant appendicular

Development (2021) 148, dev199790. doi:10.1242/dev.199790

muscle displayed a strikingly divergent phenotype characterized by enlarged AChR clusters. This led us to first ask whether, in the context of appendicular NMJ development, Agrin and Lrp4 act through MuSK. Indeed, we found that *musk*;*lrp4* double mutants recapitulated the *musk*-mutant phenotype because they failed to cluster AChRs and display axon overgrowth, confirming that Lrp4 acts through MuSK in NMJ development in appendicular muscle (Fig. 7A,B).

Given that MuSK is necessary for AChR clustering in the pectoral fin in both WT and *lrp4* mutants, and MuSK expression is sufficient to induce AChR clusters (Kim and Burden, 2008), we hypothesized that MuSK drives the formation of giant AChR clusters in the absence of *agrn* or *lrp4*. This would suggest, unexpectedly, that, in appendicular muscle, Agrin/Lrp4 restricts MuSK-dependent AChR clustering. If this were the case, we would predict that reducing MuSK expression in *lrp4* mutants would suppress the giant AChR cluster phenotype. To this end, we examined *lrp4* mutants that lacked one copy of *musk* ($lrp4^{-/-};musk^{-/+}$). Indeed, these *lrp4*-mutant animals exhibited a less-severe phenotype compared with *lrp4* homozygous mutants. Whereas fins in $lrp4^{-/-};musk^{+/-}$ larvae still contained some giant AChR clusters, portions of the fins in these animals contained smaller, evenly-dispersed neural clusters resembling the sibling patterning. Additionally, the portions of the fin with smaller AChR clusters also lacked presynaptic innervation swellings. Compared with $lrp4^{-/-}$ mutants, $lrp4^{-/-};musk^{+/-}$ mutants displayed an increase in the number of α-Btx-positive AChR clusters per fin (Fig. 7E), a rescue of the median cluster size (Fig. 7F) and a rescue of the overall distribution of cluster sizes in the fin (Fig. 7G).

In $lrp4^{-/-};musk^{+/-}$ pectoral fins, smaller clusters were mostly present in the distal fin, where AChR clusters formed later in development (Fig. S10). In contrast, 'non-rescued' giant clusters often formed closer to the proximal fin base where, during development, the first prepatterned AChR clusters emerge (Fig. 7D). This further supports the idea that Agrin/Lrp4 signaling restrains MuSK-dependent prepatterned AChR cluster growth within appendicular muscle.

Agrin/Lrp4 signaling switches MuSK from a prepatterning to an axon-induced clustering state

To further explore the idea that, unlike in axial muscle, Agrin restrains MuSK-dependent cluster growth in appendicular NMJ development, we examined the progression of appendicular NMJ development in siblings and *agrn* mutants. We predicted that, prior to the arrival of motor axons, the Agrin-independent formation of aneural prepatterned AChR clusters would be indistinguishable between siblings and *agrn* mutants. Indeed, we found that, at 46 hpf (long-pec stage), *agrn*-mutant fins exhibited prepatterned AChR clusters, indistinguishable from controls (Fig. 8A). Moreover, similar to sibling controls, navigating axons in *agrn* mutants tended to occupy the prepatterned region near the proximal fin prior to extending towards the distal fin (Fig. 8B). Subsequently, in siblings, the arrival of motor axons and the release of Agrin induced the formation of small neural clusters, akin to the process previously described in axial muscle (Panzer et al., 2006).

If nerve-derived Agrin indeed restrains prepatterned cluster growth, we predicted that, in *agrn* mutants, these initially aneural clusters would grow over time, despite the arrival of motor axons. We also predicted that lack of Agrin-mediated local MuSK activation would result in the failure to form new small neural clusters that normally emerge along growing axons. Indeed, at 60 hpf, there was a prominent difference in cluster size, number and distribution between genotypes. In siblings, the AChR cluster field mirrored the innervation pattern; even the furthest-reaching axons were associated with small AChR clusters, suggesting that, as axons grow, new clusters are rapidly formed. In contrast, in *agrn* mutants, AChR clusters had increased in size and remained globular (Fig. 8C). Unlike in siblings, presynaptic swellings apposed to AChR clusters become apparent by 72 hpf in *agrn* mutants, with stretches of axon deprived of any discernible AChR clusters (Fig. 8D). This supports the idea that navigating growth cones are inappropriately attracted to, and sequestered by, these prepatterned 'islands'. Between 72 and 120 hpf, both sibling and mutant axons continued to grow to occupy the entire muscle territory. In siblings, the majority of the AChR clusters remained small (<5 μm^2) and evenly dispersed throughout the appendicular muscle. In contrast, both presynaptic axonal swellings and neural AChR clusters continued to grow throughout the entire appendicular muscle in *agrn* mutants (Fig. 8D-F). Thus, lack of *agrn* leads to a progressive size increase in prepatterned AChR clusters. Together, our results support a model for appendicular NMJ development in which Agrin/Lrp4 signaling, in addition to its sole role in axial muscle to activate MuSK and promote NMJ development, also restrains MuSK-dependent prepatterning to size and pattern neuromuscular synapses appropriately.

DISCUSSION

The mouse diaphragm and the larval zebrafish trunk are powerful *in vivo* models to study neuromuscular synapse development. Genetic studies using these models have converged on an evolutionarily conserved pathway in which axonally released Agrin binds its receptor Lrp4 to locally activate the receptor tyrosine kinase MuSK and cluster AChRs. Here, we used the larval zebrafish pectoral fin as a genetically tractable system in which to study neuromuscular development in appendicular muscle. We report that Agrin, Lrp4 and MuSK are required to form neural AChR clusters in appendicular muscle, similar to their roles in axial muscle. In addition, we provide compelling *in vivo* evidence that Agrin and Lrp4 play an additional, previously unappreciated role to suppress the growth of aneural AChR clusters selectively in appendicular muscle. In addition, we show that Agrin/Lrp4 signaling influences presynaptic axonal patterning, because multiple axons inappropriately innervated these giant AChR clusters in *lrp4* and *agrn* mutants. Thus, our work reveals similarities and differences in the regulation of neuromuscular synapse development between two major divisions of the muscular system.

Key differences between axial versus and appendicular NMJ development

Compared with the neuromuscular system in axial muscle, little is known about either the steps by which the intricate innervation pattern of appendicular muscle arises or the genetic pathways that control this process. Our work reveals key differences in neuromuscular synapse development between axial muscle in the zebrafish trunk and appendicular muscle in the pectoral fin. First, innervation of the trunk myotome occurs much earlier than that of the pectoral fin; trunk motor axon outgrowth begins at 16 hpf (Panzer et al., 2006), whereas we first observed axon sorting at the fin plexus around 46 hpf. Second, both trunk and pectoral fin musculature were prepatterned with MuSK-dependent aneural AChR clusters. Surprisingly, prepatterned AChR clusters only form on adaxial, slow muscle fibers in the trunk (Flanagan-Steet et al., 2005; Panzer et al., 2006), and have not been reported in fast muscle fibers of the trunk, whereas, in the pectoral fin, which lacks slow muscle fibers, prepatterned AChR clusters formed exclusively

Development (2021) 148, dev199790. doi:10.1242/dev.199790

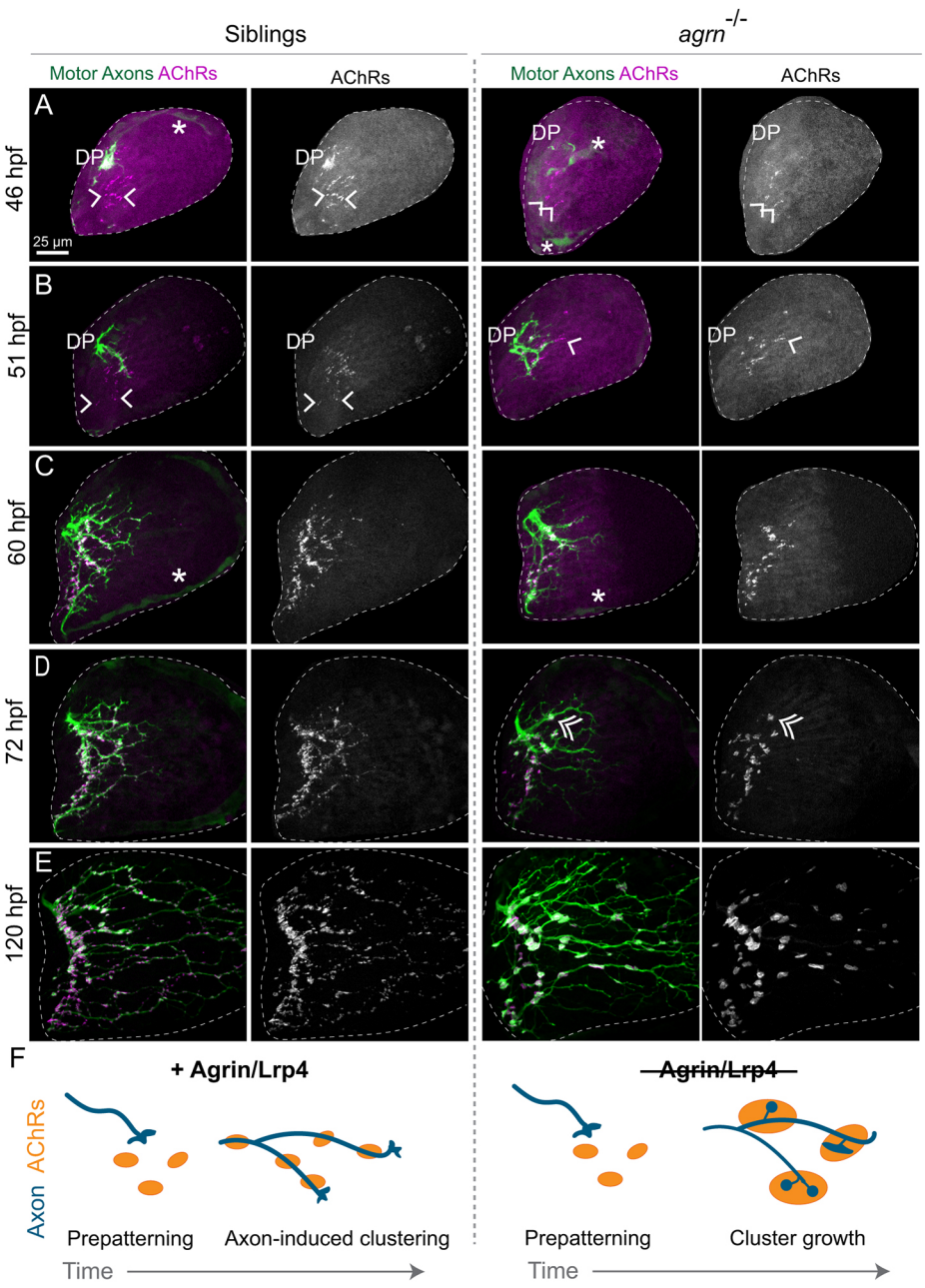

Fig. 8. Agrin restricts presynaptic terminal and neural AChR cluster size. (A-E) Developmental time course from *Tg(mnx1:GFP)* larvae with motoneurons stained with α-Btx to label AChRs. (A,B) At 46 and 51 hpf, axons growing from the dorsal plexus (DP) have not yet innervated all prepatterned AChR clusters (single arrowheads). (C-E) Whereas small clusters are added as axons grow into the pectoral fin in sibling animals, clusters mainly increase in size in *agrn* mutants. Double arrow in D indicates presynaptic swelling colocalized with an AChR cluster. Only abductor innervation is shown, with the fin area outlined by the white-dashed line. Asterisks indicate endothelial or endoskeletal cells labeled in the green channel. (F) Schematic summarizing the developmental time course. Both siblings and *agrn* mutants look similar during the prepatterning stage. Incoming axons induce small AChR clusters in sibling animals, whereas, in *agrn* mutants, AChR clusters and axonal swellings increase in size over time. *n*=4-10 animals per genotype per time point.

on fast muscle fibers. This demonstrates that both slow and fast muscle fibers have the capacity to develop AChR prepatterning, and a crucial next step will be to identify mechanisms that selectively promote AChR prepatterning in trunk slow muscle and/or suppress it in adjacent fast muscle fibers. Third, in both zebrafish trunk and mouse diaphragm muscle, prepatterned AChRs are restricted to the central region of muscle fibers. We found that AChR prepatterning in pectoral fins was also restricted, but to the proximal region of individual muscle fibers. Without the ability to track AChR clusters in live animals, we cannot exclude the possibility that prepatterned AChR clusters initially arise in the ‘center’ of nascent pectoral fin muscle fibers and, as these fibers elongate, clusters become off-center and shift towards the proximal region of muscle fibers. Independent of this possibility, our analysis of appendicular NMJ development reveals that AChR prepatterning is not strictly restricted to the center but instead can localize to other muscle fiber areas.

Finally, early motor axon outgrowth in axial muscle is confined to the center muscle fibers, in which growth cones contact prepatterned AChR clusters that form in this region (Panzer et al., 2006). Similarly, we found that, during appendicular NMJ development time points, extending axons selectively grew towards AChR prepatterned muscle regions (Fig. 8). Yet, beyond the prepatterned region, axons in the pectoral fin formed intricate patterns across muscle fibers. This growth pattern is more similar to later axon outgrowth in the trunk in which motor axons branch to innervate fast muscle fibers deep in the myotome (Beattie, 2000). These differences in prepatterning and axon outgrowth might be a consequence of the anatomy of the pectoral fin, in which axons converge at a dorsal or ventral plexus prior to topographically innervating longitudinal muscle fibers. Indeed, pectoral fin neuroanatomy is similar to that of the muscles of tetrapod forelimbs, in which axons sort at the brachial plexus to innervate distinct muscles. Although we identified a conserved requirement for MuSK to establish prepatterning across muscles,

Development (2021) 148, dev199790. doi:10.1242/dev.199790

these key anatomical and developmental differences between appendicular and axial muscles indicate that the signals that determine the location of AChR prepatterning and direct axon pathfinding are differentially regulated in appendicular muscle, leading to open questions regarding additional molecular mechanisms and pathway components that orchestrate NMJ development selectively in appendicular muscle.

Presynaptic axon patterning in appendicular muscle

Navigating growth cones respond to local extrinsic cues to determine where to form a synapse. This 'stop signal' requires MuSK signaling, because *musk* mutants in mouse and fish have an overgrown, defasciculated axon pattern (DeChiara et al., 1996; Zhang et al., 2004; Kim and Burden, 2008). In the zebrafish, the role of MuSK in axon patterning is independent of AChR clustering, because *rapsyn* mutants that lack clustered AChRs have normal axon patterning (Zhang et al., 2004; Gribble et al., 2018) (Fig. S2). Thus, MuSK independently clusters AChRs postsynaptically and regulates axon patterning, although the mechanism is poorly understood. Unexpectedly, we found that, in the pectoral fin, the presynaptic consequence of *agrn* or *lrp4* loss is for multiple axons to form mature synapses in apposition to giant postsynaptic AChR clusters, suggesting an overactive 'stop signal' in these regions. These giant clusters might reflect local 'islands' of enhanced MuSK activity, because depletion of *musk* suppressed the formation of presynaptic swellings and giant AChR clusters. Taken together, these results suggest that Lrp4 signaling, induced by the arrival of axonally released Agrin, inhibits the MuSK-dependent 'stop signal' in the appendicular muscle of the pectoral fin. Such a mechanism could be a way to signal to new waves of navigating growth cones that this synaptic region is occupied.

A dual role for Agrin/Lrp4 signaling in appendicular neuromuscular synapse development

Consistent with previous work, we found that loss of Agrin or Lrp4 led to a significant reduction in neural AChR clusters on appendicular muscle fibers, demonstrating a crucial and conserved role for both genes in promoting the formation of synaptic AChR clusters (Fig. 5C and 6D). Examining *agrn*/*lrp4* mutants and nerve-deprived pectoral fins revealed a previously unappreciated role for Agrin/Lrp4 signaling. Whereas appendicular muscle fibers lacking Agrin or Lrp4 displayed a reduced number of neural AChR clusters, the clusters that formed were significantly larger. A developmental time course is consistent with the notion that these giant clusters are derived from MuSK-dependent prepatterned AChR clusters, which, in the absence of Agrin/Lrp4 signaling, expand over time. Combined, our findings strongly support the idea that Agrin and Lrp4 play a dual role to both promote the formation of axon-induced AChR clusters and, unexpectedly, constrain the growth and development of MuSK-dependent aneural clusters into synapse-associated AChR clusters.

One attractive mechanism for how MuSK might fulfil this dual role is through Wnt signaling. MuSK can bind Wnts through its extracellular cysteine-rich domain (CRD) (Jing et al., 2009; Strochlic et al., 2012; Zhang et al., 2012). Indeed, in axial muscle of the zebrafish trunk, Wnt4a and Wnt11r binding through the MuSK CRD are required for AChR prepatterning and axon guidance (Jing et al., 2009; Gordon et al., 2012). Although a functional role for Wnt:MuSK signaling to establish prepatterning in mouse is more controversial (Messéant et al., 2015; Remédio et al., 2016), Wnt proteins in mammals regulate both AChR clustering (Henriquez et al., 2008; Wang et al., 2008) and axon guidance (reviewed by Zou, 2004). Interestingly, given that the MuSK CRD domain can adopt two distinct conformations with differential abilities to bind Wnts (Stiegler et al., 2006), Guarino et al. speculate that Agrin/Lrp4 binding to MuSK can promote a conformational change that renders MuSK unable to bind Wnts, thereby shifting downstream MuSK signaling (Guarino et al., 2020). Therefore, it is tempting to speculate that, prior to axon innervation of appendicular muscle in the pectoral fin, MuSK:Wnt signaling promotes prepatterning of both AChRs and local extracellular matrix (ECM) cues to restrict navigating growth cones to future synaptic sites. Once an axon arrives, Agrin binding to Lrp4 induces a conformational change in MuSK, preventing Wnt binding. Given that there are 23 Wnts in the zebrafish genome (Lu et al., 2011) with dynamic and differential expression throughout larval development, relevant Wnt ligands are expected to be expressed in the pectoral fin but not in the trunk. Future studies will be necessary to identify the precise upstream and downstream signaling events that enable Agrin/Lrp4 signaling to simultaneously potentiate and attenuate MuSK signaling in appendicular muscle at different regions on the same muscle fiber.

One obvious question is how Agrin/Lrp4/MuSK signaling differs between axial and appendicular muscle. At the molecular level, it appears likely that either axial muscle in the trunk is exposed to an unknown signal (redundant with Agrin/Lrp4) that attenuates MuSK-dependent prepatterning or that the appendicular muscle in the fin is exposed to a signal that potentiates MuSK-dependent prepatterning. Independently of the underlying mechanism, our results uncover a novel role for Agrin/Lrp4 signaling in modulating MuSK-dependent AChR clustering in appendicular muscle. At a broader level, the noncanonical nature of our findings reveal diversity in the molecular pathways that mediate vertebrate neuromuscular synapse development and highlight zebrafish as a powerful model to study this process beyond axial muscle.

MATERIALS AND METHODS

Zebrafish strains and animal care

Protocols and procedures involving zebrafish (*Danio rerio*) were in compliance with the University of Pennsylvania Institutional Animal Care and Use Committee regulations. All transgenic lines were maintained in the Tübigen or Tupfel long fin genetic background and were raised as previously described (Mullins et al., 1994). The following transgenic lines were used: *Tg(mnx1:GFP)*^{ml2} (Flanagan-Steet et al., 2005), *Tg(α-actin:Lrp4-GFP)*^{p159Tg} (Gribble et al., 2018), *Tg(Xla.Tubb:DsRed)*^{zf148} (Peri and Nüsslein-Volhard, 2008), *Gt(dmd-citrine)*^{ct90a} [a kind gift from Dr Sharon Amacher (The Ohio State University, Columbus, OH, USA)] (Ruf-Zamojski et al., 2015) and *Tg(α-actin:GFP)* (Higashijima et al., 1997). The following mutant strains were used: *agrn*^{p168} (Gribble et al., 2018), *lrp4*^{p184} (Remédio et al., 2016), *lrp4*^{mi36} (Saint-Amant et al., 2008), *musk*^{tbb72} (Granato et al., 1996; Zhang et al., 2004) and *rapsyn* (*two*^{th26}) (Ono et al., 2002). Mutants homozygous for these genes can be phenotyped at ∼36 hpf because they all display motor defects when prodded with a probe. The *lrp4*^{p184}, *two*^{th26} and *agrn*^{p168} alleles were genotyped using Kompetitive Allele Specific PCR (KASP, LGC Biosearch Technologies). Animals were staged as previously published (Grandel and Schulte-Merker, 1998; Kimmel et al., 1995). Within all experiments, sibling animals from the same crosses were compared following genotypic and/or phenotypic analysis. Given that our experiments in larval zebrafish occurred prior to sex determination, sex was not a relevant biological variable in this study (Kossack and Draper, 2019).

Whole-mount immunohistochemistry and imaging

Zebrafish embryos or larvae were immobilized with tricaine (A5040, Sigma-Aldrich, MS-222) and then fixed for 1 h at room temperature in sweet fix (4% paraformaldehyde with 125 mM sucrose in PBS) plus 0.1%

Development (2021) 148, dev199790. doi:10.1242/dev.199790

Triton X-100 (Fisher, BP151). The embryos or larvae were then washed in phosphate buffer and incubated overnight at 4°C in either primary chicken anti-GFP antibodies (1:2000, Aves Labs, GFP-1010) or mouse anti-Znp-1 antibodies (1:200, Developmental Studies Hybridoma Bank, AB_2315626) in incubation buffer [2 mg/ml bovine serum albumin (BSA; Sigma-Aldrich, A2153), 0.5% Triton X-100 (Thermo Fisher Scientific, BP-151), 1% normal goat serum (S-1000, Vector Laboratories)]. After washing in phosphate buffer, animals were incubated overnight at 4°C in Alexa Fluor 488 donkey anti-chicken secondary antibodies (1:1000, Jackson ImmunoResearch, 703-545-155), Alexa Fluor 594 goat anti-mouse secondary antibody (1:1000, Invitrogen, A-21125) and/or α-Btx Alexa Fluor 594 conjugate (1:500, Thermo Fisher Scientific, B13423) in incubation buffer. Animals were then mounted in agarose in a glass-bottomed dish and imaged in 1.5 µm slices using a 40× or 63× water immersion lens on a Zeiss LSM880 confocal microscope using Zen Software (Fig. 2C and 8) or a 40× water immersion lens on an ix81 Olympus spinning disk confocal microscope using SlideBook Software. The representative images within each figure include only sibling animals that were fixed and immunostained in parallel.

Sparse neuronal labeling

A DNA vector encoding *mnx1:mKate* was injected as previously described (Gribble et al., 2018; Thermes et al., 2002) into one-cell-stage embryos. Embryos were screened at 1 dpf for sparse mKate expression in the anterior spinal cord. At 5 dpf, animals were mounted in agarose and imaged live with a 40× lens using an Olympus spinning disk confocal microscope if they had sparse mKate-expressing axons innervating the pectoral fin.

Time-lapse imaging

Embryos expressing both *α-actin:GFP* and *Xla.Tubb:DsRed* were anesthetized with tricaine and mounted in agarose at around 35 hpf. Animals were time-lapse imaged with a 40× lens using an ix81 Olympus spinning disk confocal microscope in a temperature chamber set to 28°C as previously described (Rosenberg et al., 2012). Stacks through the developing fin bud were captured in 1.5 µm slices at 30 min intervals. Animals were imaged continuously for up to 3 days, with some adjustments to account for drifting and the pectoral fin moving out of frame.

Motoneuron ablation

mnx1:GFP animals were mounted in agarose and motoneurons from spinal cord segments 3-5 were ablated using an Ablate! 532 nm attenuable pulse laser (3i Intelligent Imaging Innovations) beginning at 2 dpf, prior to axons innervating the pectoral fin bud. Neurons were considered ablated when there were no GFP+ cell bodies present in the ablated spinal cord region and axons showed signs of fragmentation. Ablation was repeated at 3 dpf to prevent any regenerated motoneurons from innervating the fin. Fins were visually inspected to confirm the absence of GFP+ motor axon signals within the denervated region of the fin. Animals were fixed and stained with α-Btx at 5 dpf.

Electron microscopy

At the time of fixation, 5 dpf *lrp4* and sibling larvae were immobilized with tricaine and tails were removed for genotyping, whereas the anterior portion of the larvae was fixed with 2.5% glutaraldehyde, 2.0% paraformaldehyde in 0.1 M sodium cacodylate buffer, pH 7.4, overnight at 4°C. After washing for 10 min in 0.1 M sodium cacodylate buffer, the samples were post-fixed in 2.0% osmium tetroxide for 1 h at room temperature and then rinsed twice in distilled water prior to *en bloc* staining with 2% uranyl acetate. After dehydration through a graded ethanol series, the tissue was infiltrated and embedded in EMbed-812 (Electron Microscopy Sciences). Thin sections were stained with uranyl acetate and lead citrate and examined with a JEOL-JEM 1010 electron microscope fitted with a Hamamatsu digital camera and AMT Imaging Advantage image capture software.

Image processing and quantification

To simplify data visualization and quantification, signal from abductor or adductor innervation was manually separated from stacks through pectoral fins. Individual channel image stacks were opened in Fiji (Schindelin et al., 2012), the background was subtracted, the channels were merged and the image was changed to RGB. Stacks were visualized using the 3D viewer plugin and rotated to a top-down view so that the separation between abductor and adductor innervation was distinct. Axon signal from the opposite innervation field and other fluorescent signal from the larval body wall were selected and filled, resulting in the corresponding region filled with black on the RGB stack. Any residual signal from the opposing innervation field or trunk was removed directly on the RGB stack. This resulted in signal specific to either the abductor or adductor muscles, as specified. Stacks were converted to maximum projections. For quantification of α-Btx puncta, a custom CellProfiler (Lamprecht et al., 2007) pipeline was created to detect and measure the area of α-Btx punta per fin. Mutants that did not form distinct α-Btx puncta (*musk* and *rapsyn*) could not be quantified using CellProfiler pipelines. Fin images were excluded from analysis if the maximum projection did not include the whole fin, the fin was damaged or abnormally small, or if measurements were clear outliers from other fins of the same genotype in the dataset. For analysis of α-Btx cluster size relative to fin position (Fig. S10), the *x*-axis pixel position for the center point of clusters was binned. The area of all individual clusters in each bin was averaged. All figures show only abductor innervation except for early developmental stages in Figs 2 and 7, which are a maximum projection of the entire pectoral fin bud or elsewhere, as noted.

Statistical analysis

Data were imported into GraphPad Prism for statistical analysis. Groups were compared using an unpaired *t*-test or one-way ANOVA with either Dunnett's or Sidak's multiple comparisons tests. For histograms of cluster sizes, the area of all AChR clusters measured in each genotype were pooled and binned into 5 µm^2 bins, with any cluster over 20 µm^2 included in the same bin. Distributions were compared using a Kruskal–Wallis test with Dunn's multiple comparisons test. In figures in which the control group is labeled as 'siblings', we pooled WT and heterozygous animals because there was no statistical difference between these groups.

Acknowledgements

The authors thank members of the Granato lab for helpful feedback on the manuscript. Finally, we thank the Penn Sanger sequencing core, the Penn Cell and Developmental Biology microscopy core, and the Electron Microscopy Resource Lab.

Competing interests

The authors declare no competing or financial interests.

Author contributions

Conceptualization: L.J.W., M.G.; Methodology: L.J.W.; Validation: L.J.W., R.A.R.; Formal analysis: L.J.W.; Investigation: L.J.W., R.A.R., M.F.N.; Data curation: L.J.W.; Writing - original draft: L.J.W.; Writing - review & editing: L.J.W., M.G.; Visualization: L.J.W.; Supervision: L.J.W., M.G.; Project administration: M.G.; Funding acquisition: L.J.W., M.G.

Funding

This work was supported by the National Institutes of Health (K01NS119496 and F32 NS103219 to L.J.W., R01NS097914 and RO1 EY024861 to M.G.). Deposited in PMC for release after 12 months.

References

Beattie, C. E. (2000). Control of motor axon guidance in the zebrafish embryo. *Brain Res. Bull.* **53**, 489-500. doi:10.1016/S0361-9230(00)00382-8

Bekoff, A. and Betz, W. J. (1976). Acetylcholine hot spots: development on myotubes cultured from aneural limb buds. *Science* **193**, 915-917. doi:10.1126/science.948754

DeChiara, T. M., Bowen, D. C., Valenzuela, D. M., Simmons, M. V., Poueymirou, W. T., Thomas, S., Kinetz, E., Compton, D. L., Rojas, E., Park, J. S. et al. (1996). The receptor tyrosine kinase MuSK is required for neuromuscular junction formation in vivo. *Cell* **85**, 501-512. doi:10.1016/S0092-8674(00)81251-9

Eisen, J. S., Myers, P. Z. and Westerfield, M. (1986). Pathway selection by growth cones of identified motoneurones in live zebra fish embryos. *Nature* **320**, 269-271. doi:10.1038/320269a0

Flanagan-Steet, H., Fox, M. A., Meyer, D. and Sanes, J. R. (2005). Neuromuscular synapses can form in vivo by incorporation of initially aneural postsynaptic specializations. *Development* **132**, 4471-4481. doi:10.1242/dev.02044

Gillespie, S. K. H., Balasubramanian, S., Fung, E. T. and Huganir, R. L. (1996). Rapsyn clusters and activates the synapse-specific receptor tyrosine kinase MuSK. *Neuron* **16**, 953-962. doi:10.1016/S0896-6273(00)80118-X

Gordon, L. R., Gribble, K. D., Syrett, C. M. and Granato, M. (2012). Initiation of synapse formation by Wnt-induced MuSK endocytosis. *Development* **139**, 1023-1033. doi:10.1242/dev.071555

Granato, M., van Eeden, F. J., Schach, U., Trowe, T., Brand, M., Furutani-Seiki, M., Haffter, P., Hammerschmidt, M., Heisenberg, C. P., Jiang, Y. J. et al. (1996). Genes controlling and mediating locomotion behavior of the zebrafish embryo and larva. *Development* **123**, 399-413. doi:10.1242/dev.123.1.399

Grandel, H. and Schulte-Merker, S. (1998). The development of the paired fins in the Zebrafish (Danio rerio). *Mech. Dev.* **79**, 99-120. doi:10.1016/S0925-4773(98)00176-2

Gribble, K. D., Walker, L. J., Saint-Amant, L., Kuwada, J. Y. and Granato, M. (2018). The synaptic receptor Lrp4 promotes peripheral nerve regeneration. *Nat. Commun.* **9**, 2389. doi:10.1038/s41467-018-04806-4

Guarino, S. R., Canciani, A. and Forneris, F. (2020). Dissecting the extracellular complexity of neuromuscular junction organizers. *Front. Mol. Biosci.* **6**, 156. doi:10.3389/fmolb.2019.00156

Henriquez, J. P., Webb, A., Bence, M., Bildsoe, H., Sahores, M., Hughes, S. M. and Salinas, P. C. (2008). Wnt signaling promotes AChR aggregation at the neuromuscular synapse in collaboration with agrin. *Proc. Natl. Acad. Sci. USA* **105**, 18812-18817. doi:10.1073/pnas.0806300105

Higashijima, S.-i., Okamoto, H., Ueno, N., Hotta, Y. and Eguchi, G. (1997). High-frequency generation of transgenic zebrafish which reliably express GFP in whole muscles or the whole body by using promoters of zebrafish origin. *Dev. Biol.* **192**, 289-299. doi:10.1006/dbio.1997.8779

Jing, L., Lefebvre, J. L., Gordon, L. R. and Granato, M. (2009). Wnt signals organize synaptic prepattern and axon guidance through the zebrafish unplugged/MuSK receptor. *Neuron* **61**, 721-733. doi:10.1016/j.neuron.2008.12.025

Jing, L., Gordon, L. R., Shtibin, E. and Granato, M. (2010). Temporal and spatial requirements of unplugged/MuSK function during zebrafish neuromuscular development. *PLoS ONE* **5**, e8843. doi:10.1371/journal.pone.0008843

Kim, N. and Burden, S. J. (2008). MuSK controls where motor axons grow and form synapses. *Nat. Neurosci.* **11**, 19-27. doi:10.1038/nn2026

Kim, N., Stiegler, A. L., Cameron, T. O., Hallock, P. T., Gomez, A. M., Huang, J. H., Hubbard, S. R., Dustin, M. L. and Burden, S. J. (2008). Lrp4 is a receptor for Agrin and forms a complex with MuSK. *Cell* **135**, 334-342. doi:10.1016/j.cell.2008.10.002

Kimmel, C. B., Ballard, W. W., Kimmel, S. R., Ullmann, B. and Schilling, T. F. (1995). Stages of embryonic development of the zebrafish. *Dev. Dyn.* **203**, 253-310. doi:10.1002/aja.1002030302

Kossack, M. E. and Draper, B. W. (2019). Genetic regulation of sex determination and maintenance in zebrafish (Danio rerio). *Curr. Top. Dev. Biol.* **134**, 119-149. doi:10.1016/bs.ctdb.2019.02.004

Lamprecht, M. R., Sabatini, D. M. and Carpenter, A. E. (2007). CellProfiler™: free, versatile software for automated biological image analysis. *BioTechniques* **42**, 71-75. doi:10.2144/000112257

Lefebvre, J. L., Jing, L., Becaficco, S., Franzini-Armstrong, C. and Granato, M. (2007). Differential requirement for MuSK and dystroglycan in generating patterns of neuromuscular innervation. *Proc. Natl. Acad. Sci. USA* **104**, 2483-2488. doi:10.1073/pnas.0610822104

Lin, W., Burgess, R. W., Dominguez, B., Pfaff, S. L., Sanes, J. R. and Lee, K.-F. (2001). Distinct roles of nerve and muscle in postsynaptic differentiation of the neuromuscular synapse. *Nature* **410**, 1057-1064. doi:10.1038/35074025

Lu, F.-I., Thisse, C. and Thisse, B. (2011). Identification and mechanism of regulation of the zebrafish dorsal determinant. *Proc. Natl. Acad. Sci. USA* **108**, 15876-15880. doi:10.1073/pnas.1106801108

Mercader, N. (2007). Early steps of paired fin development in zebrafish compared with tetrapod limb development. *Dev. Growth Differ.* **49**, 421-437. doi:10.1111/j.1440-169X.2007.00942.x

Messéant, J., Dobbertin, A., Girard, E., Delers, P., Manuel, M., Mangione, F., Schmitt, A., Le Denmat, D., Molgó, J., Zytnicki, D. et al. (2015). MuSK frizzled-like domain is critical for mammalian neuromuscular junction formation and maintenance. *J. Neurosci.* **35**, 4926-4941. doi:10.1523/JNEUROSCI.3381-14.2015

Moody-Corbett, F. and Cohen, M. W. (1982). Influence of nerve on the formation and survival of acetylcholine receptor and cholinesterase patches on embryonic Xenopus muscle cells in culture. *J. Neurosci.* **2**, 633-646. doi:10.1523/JNEUROSCI.02-05-00633.1982

Mullins, M. C., Hammerschmidt, M., Haffter, P. and Nüsslein-Volhard, C. (1994). Large-scale mutagenesis in the zebrafish: in search of genes controlling development in a vertebrate. *Curr. Biol.* **4**, 189-202. doi:10.1016/S0960-9822(00)00048-8

Myers, P. Z. (1985). Spinal motoneurons of the larval zebrafish. *J. Comp. Neurol.* **236**, 555-561. doi:10.1002/cne.902360411

Ono, F., Shcherbatko, A., Higashijima, S.-i., Mandel, G. and Brehm, P. (2002). The zebrafish motility mutant twitch once reveals new roles for rapsyn in synaptic function. *J. Neurosci.* **22**, 6491-6498. doi:10.1523/JNEUROSCI.22-15-06491.2002

Panzer, J. A., Song, Y. and Balice-Gordon, R. J. (2006). In vivo imaging of preferential motor axon outgrowth to and synaptogenesis at prepatterned acetylcholine receptor clusters in embryonic zebrafish skeletal muscle. *J. Neurosci.* **26**, 934-947. doi:10.1523/JNEUROSCI.3656-05.2006

Patterson, S. E., Mook, L. B. and Devoto, S. H. (2008). Growth in the larval zebrafish pectoral fin and trunk musculature. *Dev. Dyn.* **237**, 307-315. doi:10.1002/dvdy.21400

Peng, H. B. (1986). Elimination of preexistent acetylcholine receptor clusters induced by the formation of new clusters in the absence of nerve. *J. Neurosci.* **6**, 581-589. doi:10.1523/JNEUROSCI.06-02-00581.1986

Peri, F. and Nüsslein-Volhard, C. (2008). Live imaging of neuronal degradation by microglia reveals a role for v0-ATPase a1 in phagosomal fusion in vivo. *Cell* **133**, 916-927. doi:10.1016/j.cell.2008.04.037

Remédio, L., Gribble, K. D., Lee, J. K., Kim, N., Hallock, P. T., Delestrée, N., Mentis, G. Z., Froemke, R. C., Granato, M. and Burden, S. J. (2016). Diverging roles for Lrp4 and Wnt signaling in neuromuscular synapse development during evolution. *Genes Dev.* **30**, 1058-1069. doi:10.1101/gad.279745.116

Rosenberg, A. F., Wolman, M. A., Franzini-Armstrong, C. and Granato, M. (2012). In vivo nerve-macrophage interactions following peripheral nerve injury. *J. Neurosci.* **32**, 3898-3909. doi:10.1523/JNEUROSCI.5225-11.2012

Ruf-Zamojski, F., Trivedi, V., Fraser, S. E. and Trinh, L. A. (2015). Spatio-temporal differences in dystrophin dynamics at mRNA and protein levels revealed by a novel fliptrap line. *PLoS ONE* **10**, e0128944. doi:10.1371/journal.pone.0128944

Saint-Amant, L., Sprague, S. M., Hirata, H., Li, Q., Cui, W. W., Zhou, W., Poudou, O., Hume, R. I. and Kuwada, J. Y. (2008). The zebrafish ennui behavioral mutation disrupts acetylcholine receptor localization and motor axon stability. *Dev. Neurobiol.* **68**, 45-61. doi:10.1002/dneu.20569

Schindelin, J., Arganda-Carreras, I., Frise, E., Kaynig, V., Longair, M., Pietzsch, T., Preibisch, S., Rueden, C., Saalfeld, S., Schmid, B. et al. (2012). Fiji: an open-source platform for biological-image analysis. *Nat. Methods* **9**, 676-682. doi:10.1038/nmeth.2019

Siomava, N., Shkil, F., Voronezhskaya, E. and Diogo, R. (2018). Development of zebrafish paired and median fin musculature: basis for comparative, developmental, and macroevolutionary studies. *Sci. Rep.* **8**, 14187. doi:10.1038/s41598-018-32567-z

Stiegler, A. L., Burden, S. J. and Hubbard, S. R. (2006). Crystal structure of the Agrin-responsive immunoglobulin-like domains 1 and 2 of the receptor tyrosine kinase MuSK. *J. Mol. Biol.* **364**, 424-433. doi:10.1016/j.jmb.2006.09.019

Strochlic, L., Falk, J., Goillot, E., Sigoillot, S., Bourgeois, F., Delers, P., Rouvière, J., Swain, A., Castellani, V., Schaeffer, L. et al. (2012). Wnt4 participates in the formation of vertebrate neuromuscular junction. *PLoS ONE* **7**, e29976. doi:10.1371/journal.pone.0029976

Thermes, V., Grabher, C., Ristoratore, F., Bourrat, F., Choulika, A., Wittbrodt, J. and Joly, J.-S. (2002). I-SceI meganuclease mediates highly efficient transgenesis in fish. *Mech. Dev.* **118**, 91-98. doi:10.1016/S0925-4773(02)00218-6

Thorsen, D. H. and Hale, M. E. (2007). Neural development of the zebrafish (Danio rerio) pectoral fin. *J. Comp. Neurol.* **504**, 168-184. doi:10.1002/cne.21425

Thorsen, D. H., Cassidy, J. J. and Hale, M. E. (2004). Swimming of larval zebrafish: fin–axis coordination and implications for function and neural control. *J. Exp. Biol.* **207**, 4175-4183. doi:10.1242/jeb.01285

Uemura, Y., Kato, K., Kawakami, K., Kimura, Y., Oda, Y. and Higashijima, S.-i. (2020). Neuronal circuits that control rhythmic pectoral fin movements in zebrafish. *J. Neurosci.* **40**, 6678-6690. doi:10.1523/JNEUROSCI.1484-20.2020

Wang, J., Ruan, N.-J., Qian, L., Lei, W.-l., Chen, F. and Luo, Z.-G. (2008). Wnt/β-catenin signaling suppresses Rapsyn expression and inhibits acetylcholine receptor clustering at the neuromuscular junction. *J. Biol. Chem.* **283**, 21668-21675. doi:10.1074/jbc.M709939200

Yang, X., Arber, S., William, C., Li, L., Tanabe, Y., Jessell, T. M., Birchmeier, C. and Burden, S. J. (2001). Patterning of muscle acetylcholine receptor gene expression in the absence of motor innervation. *Neuron* **30**, 399-410. doi:10.1016/S0896-6273(01)00287-2

Yano, T., Abe, G., Yokoyama, H., Kawakami, K. and Tamura, K. (2012). Mechanism of pectoral fin outgrowth in zebrafish development. *Development* **139**, 2916-2925. doi:10.1242/dev.075572

Zhang, J., Lefebvre, J. L., Zhao, S. and Granato, M. (2004). Zebrafish unplugged reveals a role for muscle-specific kinase homologs in axonal pathway choice. *Nat. Neurosci.* **7**, 1303-1309. doi:10.1038/nn1350

Zhang, B., Luo, S., Wang, Q., Suzuki, T., Xiong, W. C. and Mei, L. (2008). LRP4 serves as a coreceptor of agrin. *Neuron* **60**, 285-297. doi:10.1016/j.neuron.2008.10.006

Zhang, B., Liang, C., Bates, R., Yin, Y., Xiong, W.-C. and Mei, L. (2012). Wnt proteins regulate acetylcholine receptor clustering in muscle cells. *Mol. Brain* **5**, 7. doi:10.1186/1756-6606-5-7

Zong, Y., Zhang, B., Gu, S., Lee, K., Zhou, J., Yao, G., Figueiredo, D., Perry, K., Mei, L. and Jin, R. (2012). Structural basis of agrin–LRP4–MuSK signaling. *Genes Dev.* **26**, 247-258. doi:10.1101/gad.180885.111

Zou, Y. (2004). Wnt signaling in axon guidance. *Trends Neurosci.* **27**, 528-532. doi:10.1016/j.tins.2004.06.015

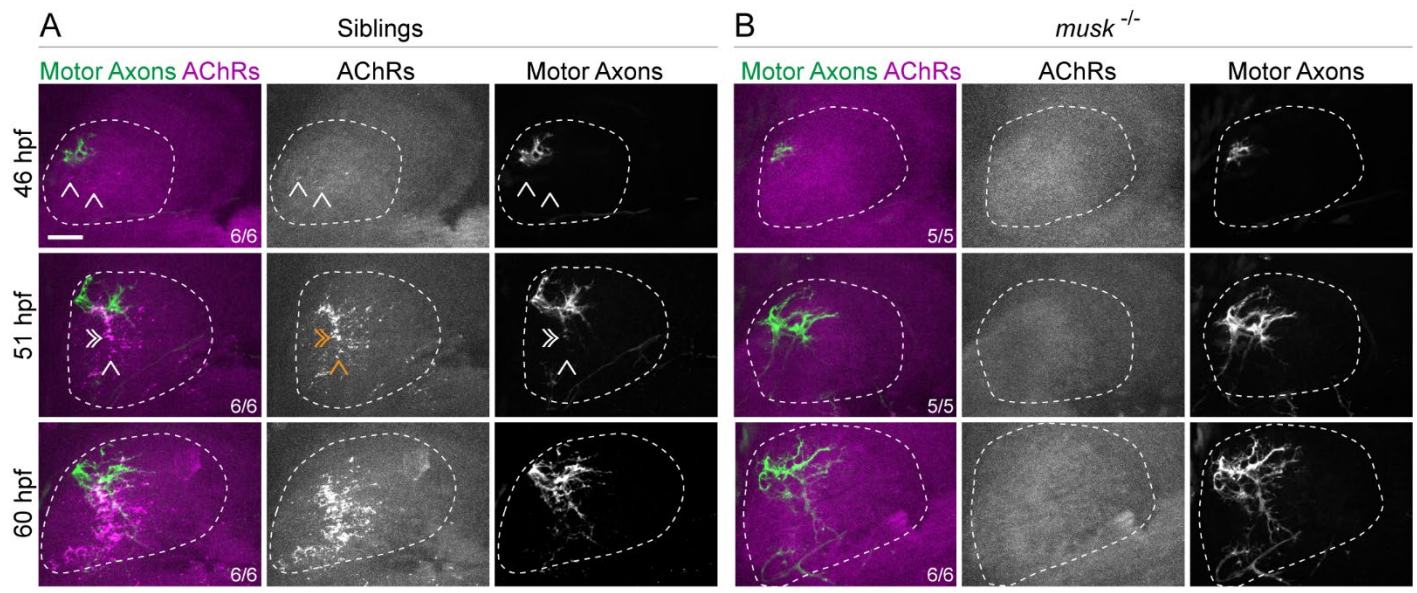

Fig. S1. Musk is required for pectoral fin prepatterning. Lateral view of maximum projections through pectoral fins of *Tg(mnx1:GFP)* larvae to label all motor neurons. Fins were stained with α-bungarotoxin to label acetylcholine receptors (AChRs). Dotted line outlines pectoral fin musculature. Single arrows point to aneural AChR clusters in siblings (A) that are absent in *musk* mutants (B). The double arrows at 51 hpf point to neural clusters. Brightness and contrast was individually adjusted across images so that background fluorescence was comparable but raw images were scored blinded. Scale bar is 25 microns.

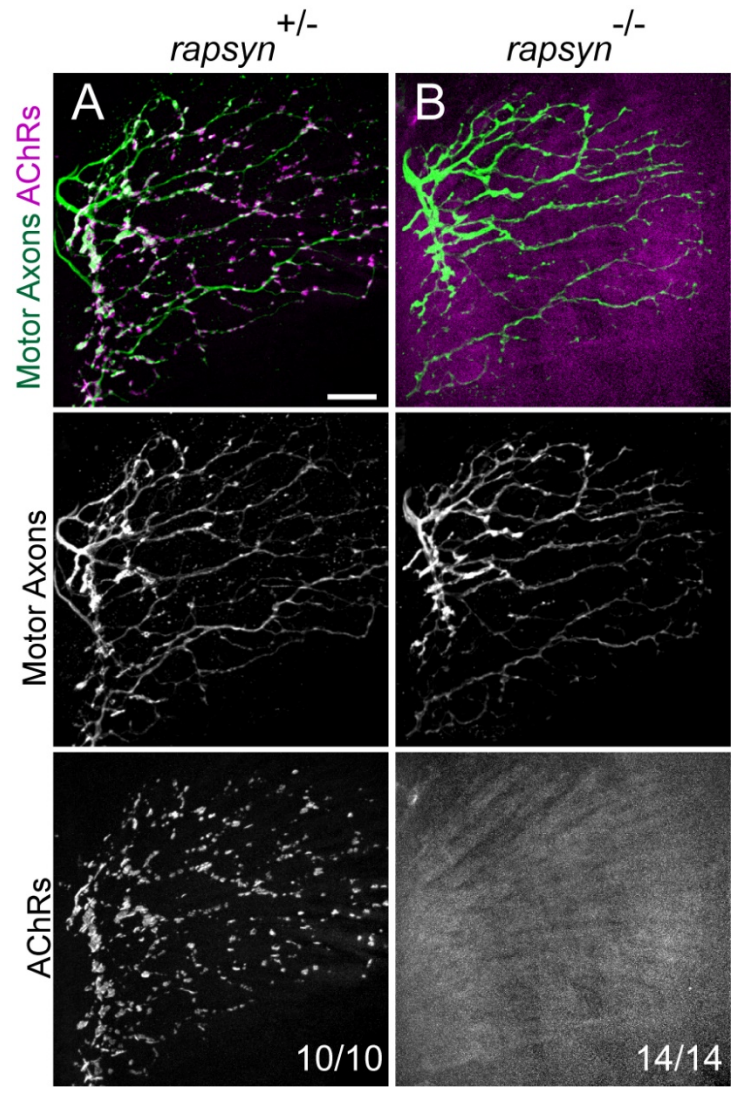

Fig. S2. Rapsyn is required for neuromuscular synapse formation. Abductor muscle innervation in the pectoral fin from 120 hours post fertilization *Tg*(*mnx1:GFP*) larvae expressing GFP to label motor neurons and stained with α-bungarotoxin to label acetylcholine receptors (AChRs). A) *rapsyn* sibling animals have numerous small AChR clusters while *rapsyn* mutants have diffuse AChR signal throughout muscle fibers in the fin. Images are maximum intensity projections. n = 10 (siblings), 14 (mutants). Scale bar is 25 microns.

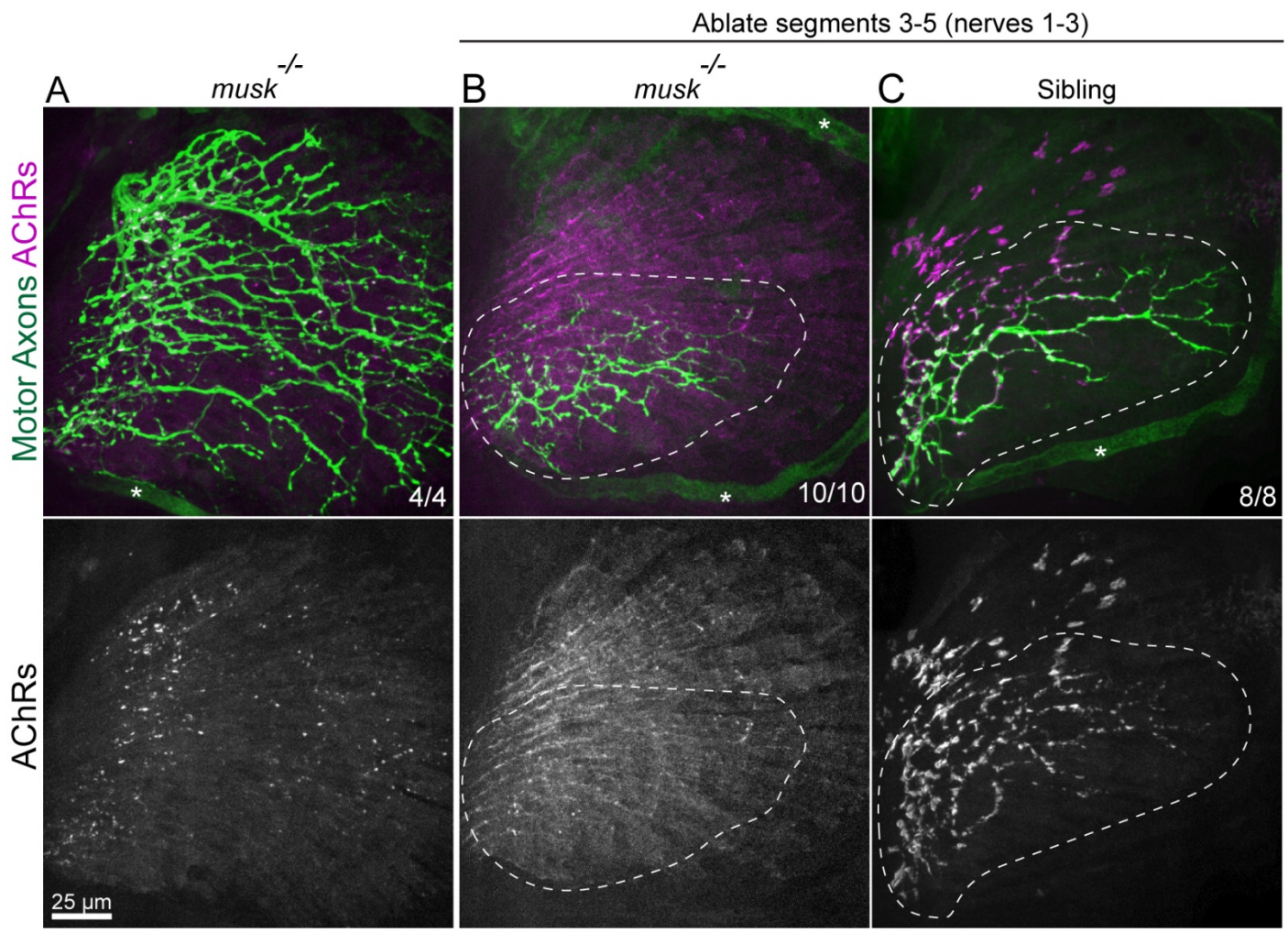

Fig. S3. MuSK is required to form large clusters in denervated pectoral fins. Spinal segments 3-5 were ablated in *Tg(mnx1:GFP)* embryos at 2, 3, and 4 dpf to prevent dorsal innervation of pectoral fins from nerves 1-3. At 5 dpf, both (A) unablated control *musk* mutant and (B) ablated *musk* mutant pectoral fins display diffuse AChR localization. C) In contrast, the non-innervated region of sibling pectoral fins displays abnormally large AChR clusters (see figure 4) while the innervated region exhibits small axon-induced AChR clusters. The innervated region in motoneuron-ablated fins is outlined in the white dotted line. The asterisks point to pectoral fin vasculature.

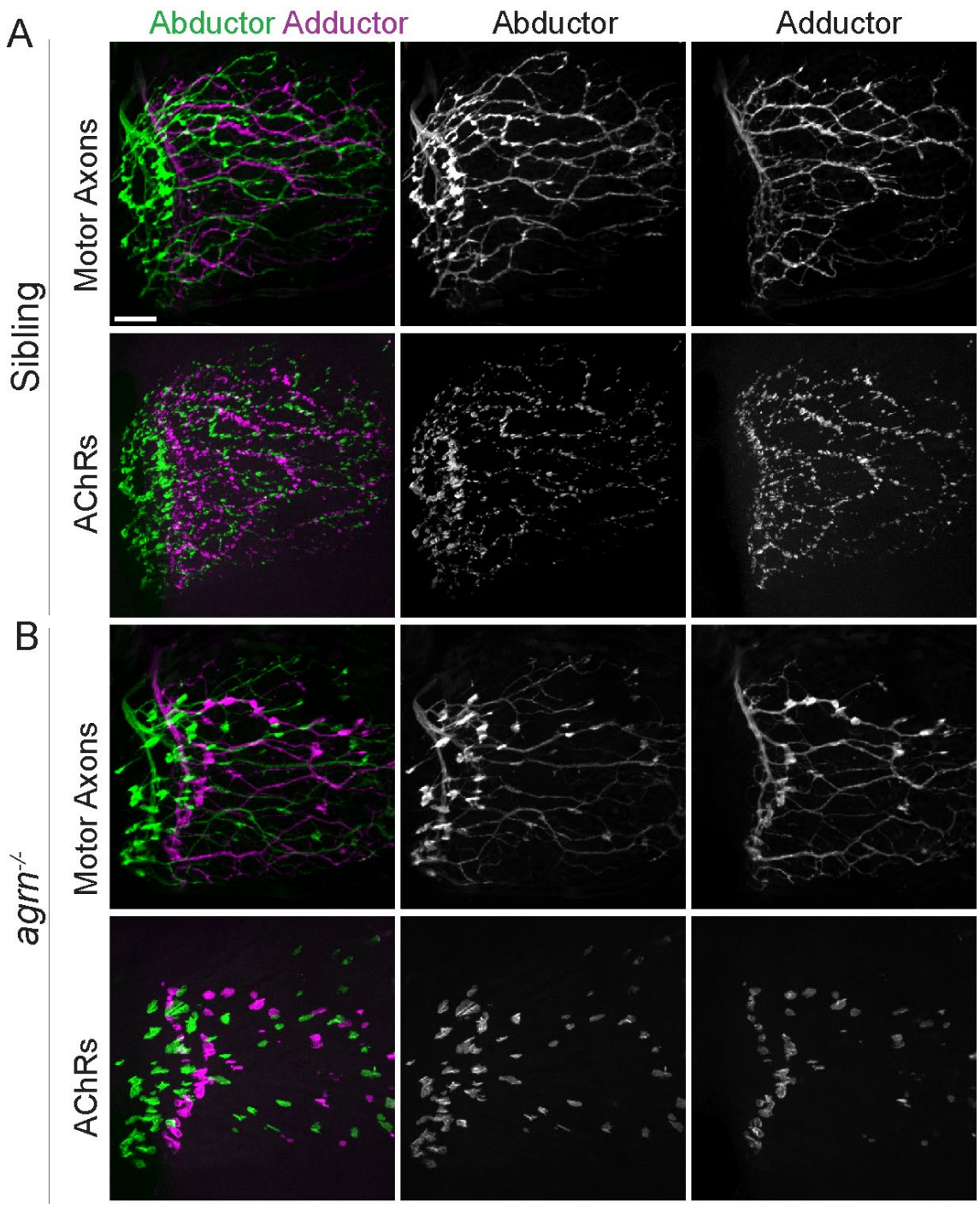

Fig. S4. Abductor and adductor muscles exhibit identical innervation phenotypes.
Tg(mnx1:GFP) pectoral fins stained with α-bungarotoxin to label acetylcholine receptors (AChRs) in siblings (A) or *agrn* mutants (B). Innervation pattern or α-bungarotoxin stain from abductor (green) or adductor (magenta) muscle pseudo-colored in merged maximum projection. Signal from each muscle is also shown individually. As the phenotype is similar between the abductor and adductor muscles, for most figures we have only shown the abductor innervation. N = 25 (siblings), 22 (mutants). Scale bar is 25 microns.

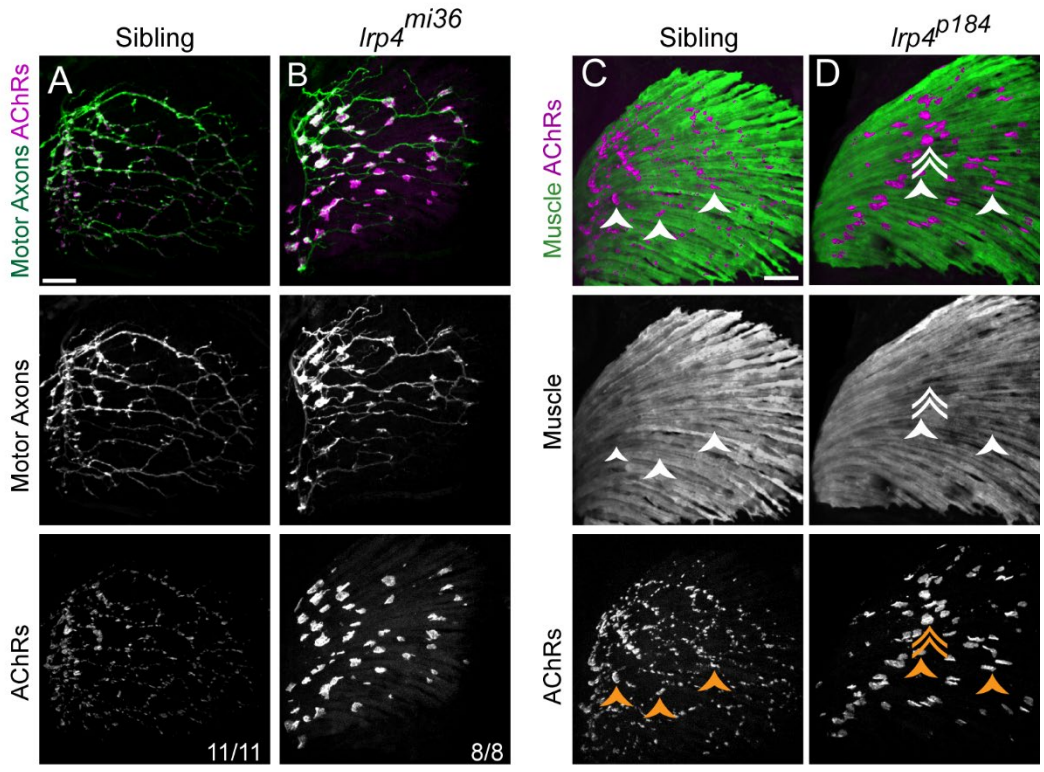

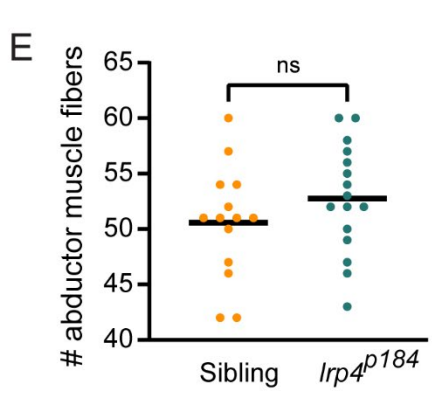

Fig. S5. Lrp4 acts through a ligand-dependent mechanism and muscles develop normally. Maximum projection of abductor innervation of 120 hours post fertilization *Tg(mnx1:GFP)* pectoral fins expressing GFP in all motor neurons and stained with α-bungarotoxin to label acetylcholine receptors (AChR). Compared with siblings (A), *lrp4*^{mi36} (ennui) mutants lacking the intracellular domain (B) have swellings in the motor neuron innervation pattern and enlarged AChR clusters, identical to presumptive null *lrp4*^{p184} mutants. Pectoral fin muscles labeled by *α-actin:GFP* are indistinguishable between siblings and *lrp4*^{p184} mutants. (C) AChR clusters labeled with α-bungarotoxin reveal hundreds of small clusters (arrowheads) distributed across muscle fibers in siblings. (D) In contrast, giant AChR clusters in *lrp4* mutants nestle between adjacent muscle fibers (arrowheads) or can span across multiple muscle fibers (double arrowhead). A minimum of 10 samples were screened per condition. Scale bars are 25 microns. (E) There is no difference in the number of abductor muscle fibers in *lrp4* mutants compared to sibling controls.

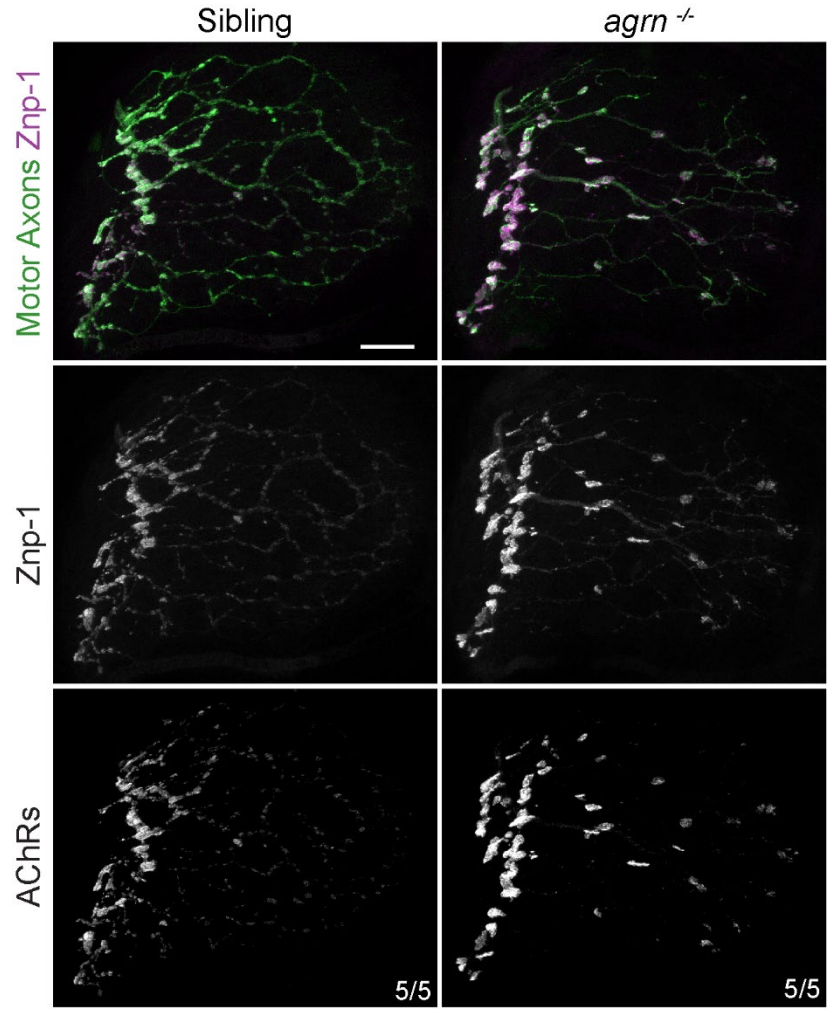

Fig. S6. Presynaptic marker Znp-1 colocalizes with AChR clusters in the pectoral fin. At 120 hours post fertilization, sibling control and *agrn* mutant pectoral fins exhibit postsynaptic AChR clusters labeled with α-bungarotoxin that colocalize with the presynaptic marker Znp-1, which labels Synaptotagmin 2. Motor axons were labeled with *mnx1:GFP*. Scale bar is 25 microns.

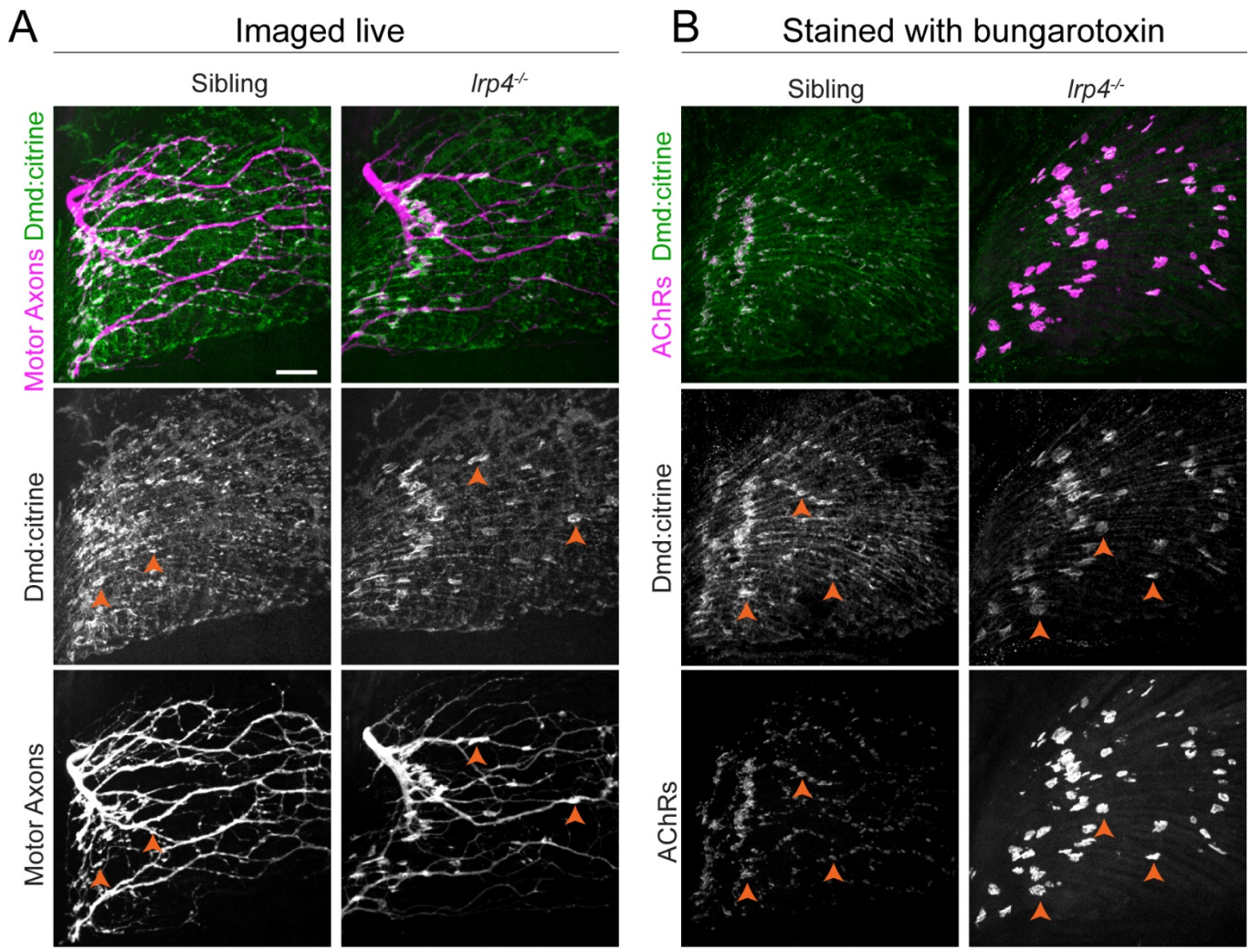

Fig. S7. Giant clusters co-localize with postsynaptic marker Dystrophin. Endogenous Dystrophin, labeled with *Gt(dmd-citrine)*, is expressed diffusely in the pectoral fin but concentrates between muscle fibers and at synaptic regions. A) Co-labeling with motor axons (labeled with *Tg(Xla.tubb:dsRed)* shows that concentrated Dmd-citrine co-localizes with axons in sibling controls and with presynaptic swellings in *lrp4* mutants. B) Dmd-citrine signal concentrates in regions marked with α-bungarotoxin to label acetylcholine receptors (AChRs) in both sibling controls and *lrp4* mutants. A minimum of 10 samples were screened per condition. Scale bar is 25 microns.

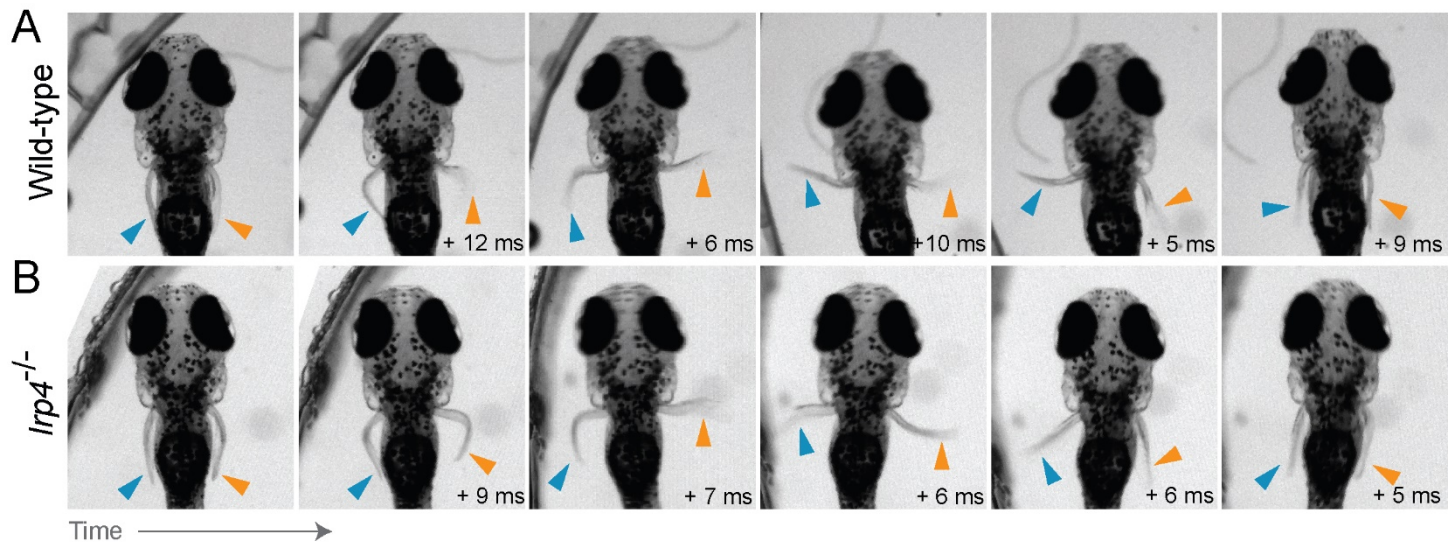

Fig. S8. Pectoral fin movements are grossly normal in *lrp4* mutants. High-speed imaging of pectoral fin movements in (A) wild-type (n=6) and (B) *lrp4* mutant (n=7) larvae at ~120 hpf. Despite their abnormal neuromuscular synapses, *lrp4* mutant pectoral fin movements are grossly normal compared to wild-type siblings. Movies were captured at 1000 frames per second. Time elapsed from the previous frame is reported in milliseconds (ms) in the bottom right of each still image. Blue arrows point to the left fin and orange arrows point to the right fin.

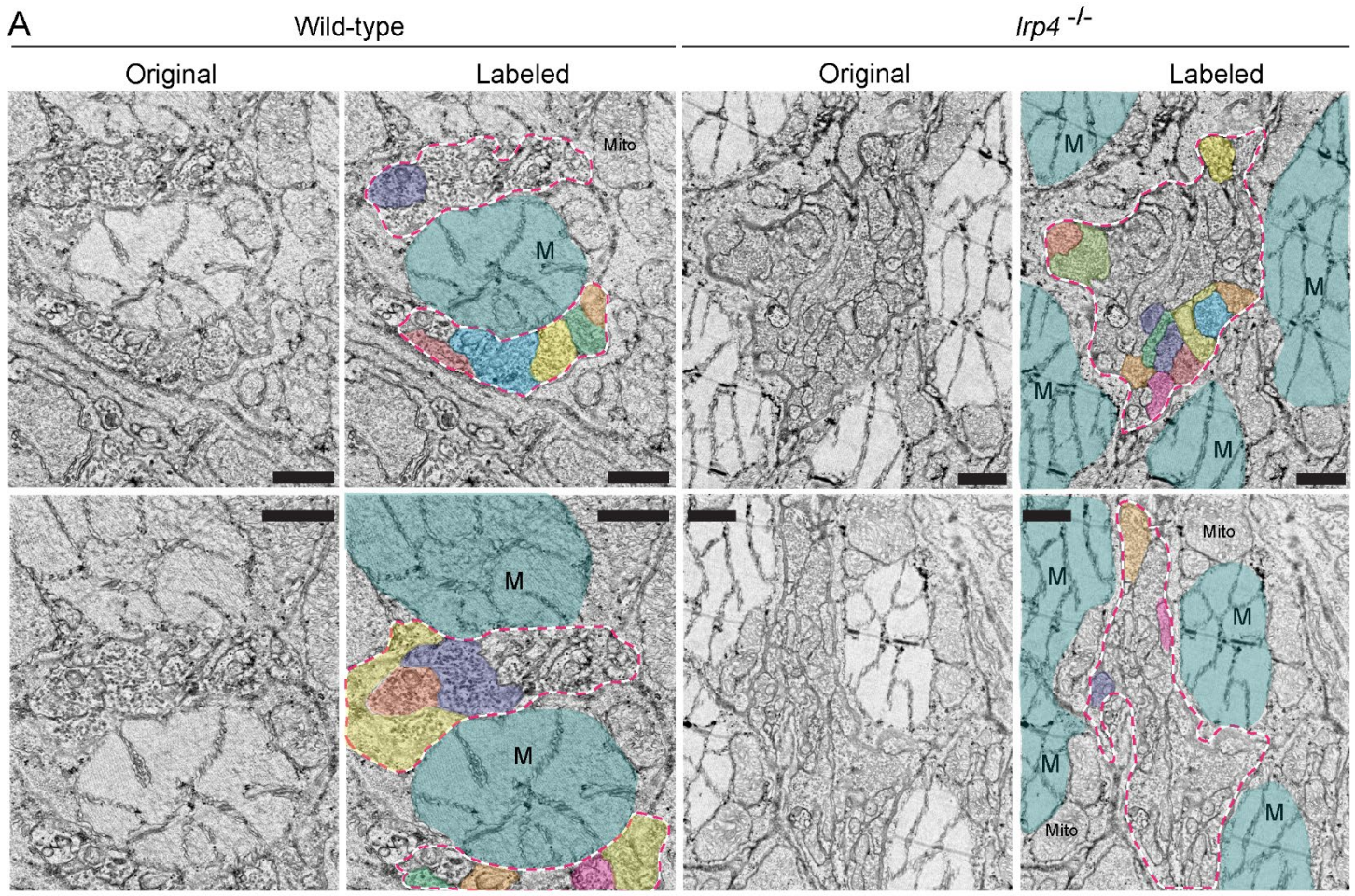

Fig. S9. Electron microscopy of pectoral fins.
A) Electron micrographs in wild-type and *lrp4* mutant pectoral fins at 5 dpf. Images are cross-sections across myofibrils. Original micrographs are shown to the left with the same micrograph pseudo-colored and labeled to the right. Some myofibrils (M) are pseudo-colored in teal and some mitochondria (Mito) are labeled. Regions with vesicle-positive axonal processes, as defined by structures with synaptic vesicles, are outlined in the pink dotted line and quantified in B. Individual vesicle-positive axonal processes are pseudo-colored in different colors when their borders could be defined. B) Quantification of the total area of each region with vesicle-positive axonal processes (pink outlined areas). The three *lrp4* mutant datapoints in magenta were cut off at the edge of the micrograph. Scale bars are 1 micron. N = 10 (wild-type) and 11 (*lrp4* mutant) regions with vesicle-positive axonal processes..

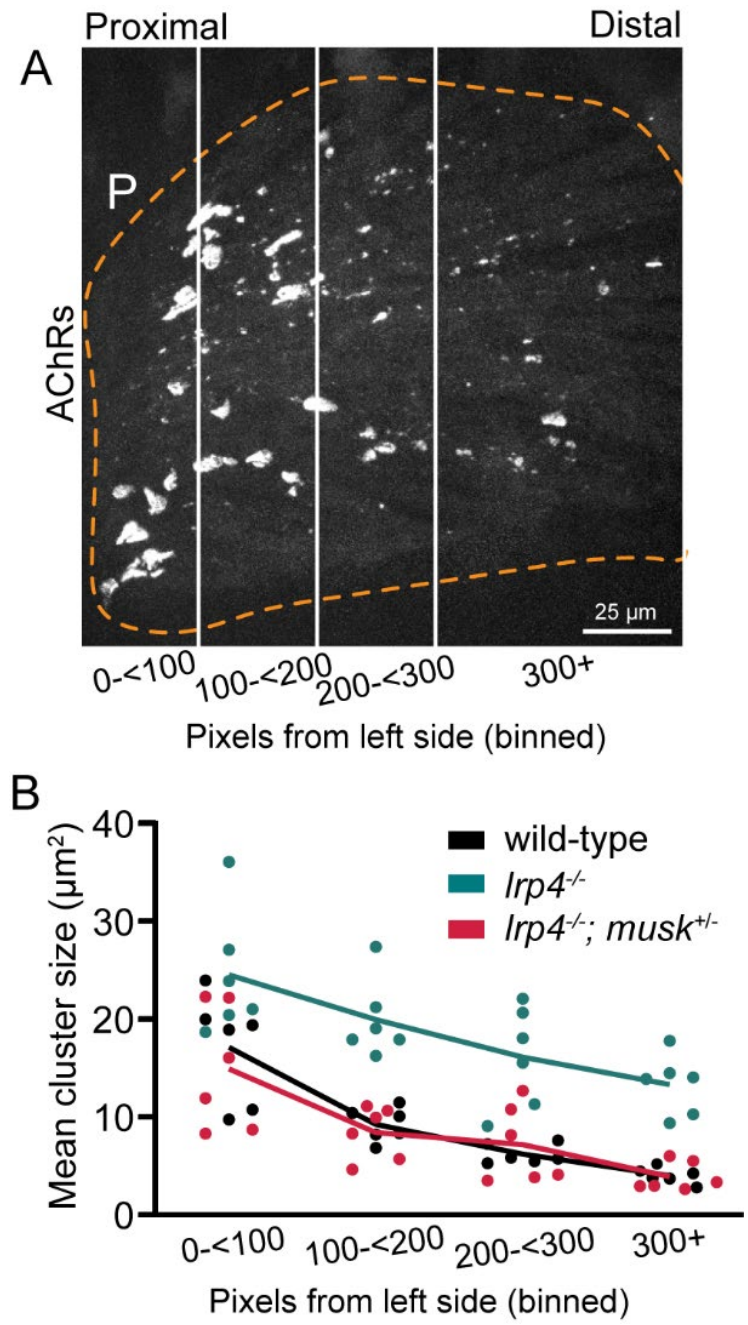

Fig. S10. Smaller AChR clusters localize to the distal tip of pectoral fins. A) Pectoral fin AChR clusters from Figure 7 were binned according to their position relative to the left side of images as shown in the example fin (from Figure 7D). The location of the dorsal plexus is marked with P. B) The mean area of individual clusters within each bin were plotted relative to their position. Each point per bin represents a different fin. Like wild-type pectoral fins, the largest AChR clusters in *lrp4* mutants that are heterozygous for *musk* (*lrp4*$^{-/-}$;*musk*$^{+/-}$) are found in the proximal fin base while smaller clusters localize to the distal fin.

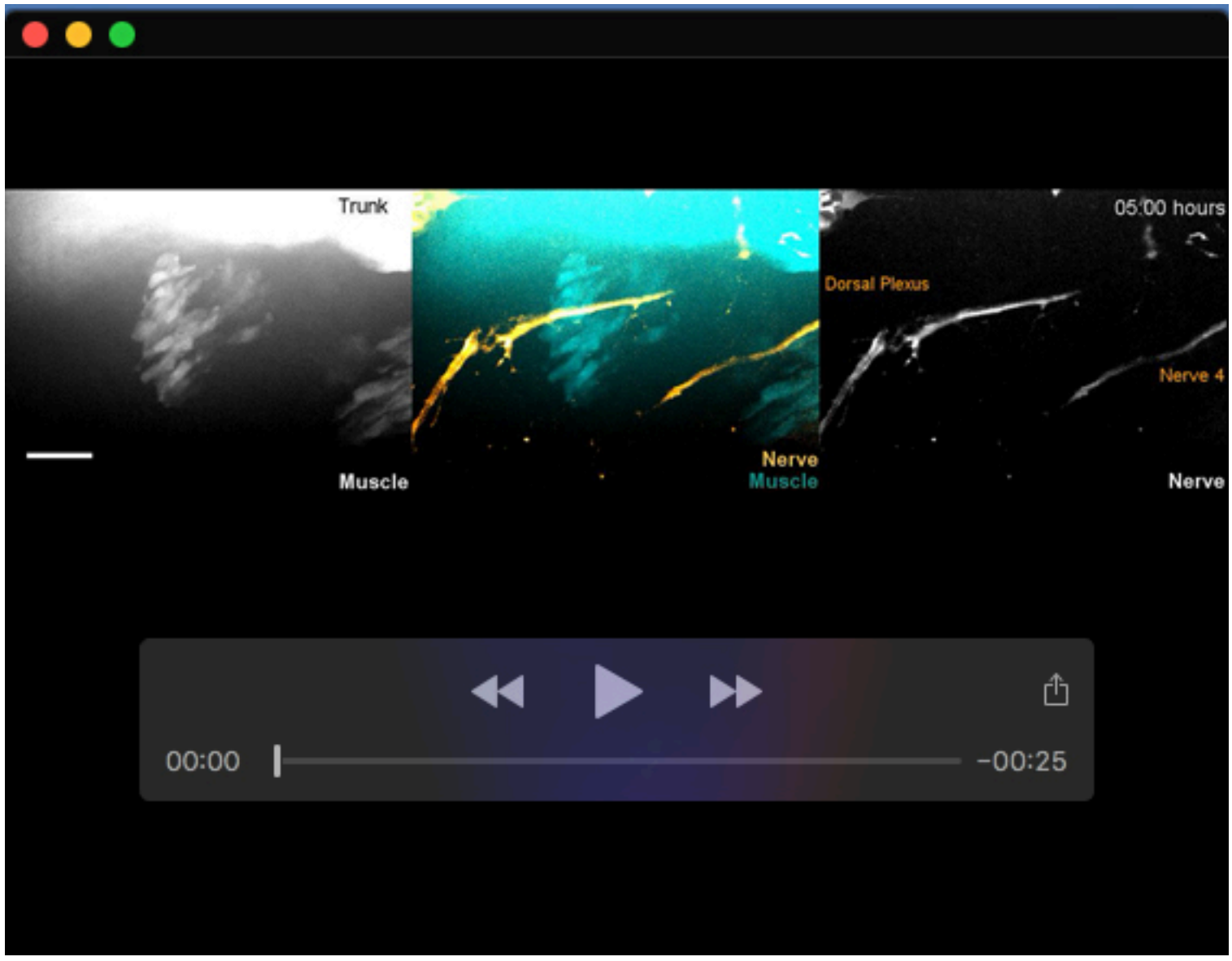

Movie 1. Timelapse of pectoral fin development. Live imaging of *Tg(α-actin:GFP); Tg(Xla.Tubb:DsRed)* larvae to label muscles and axons, respectively. By approximately prim-25 (36 hpf; start of movie), motor axons from nerves 1-3 coalesce at what will form the dorsal plexus and nascent muscle fibers in the pectoral fin bud, located laterally to the axons, have just started expressing *α-actin*:*GFP.* Muscle fibers continue to divide and reorganize through the long-pec stage as the fin moves further medial, closer to the plane of the dorsal plexus, and motor axons begin to grow into the abductor and then adductor muscles beginning around the long-pec stage (approximately 13 hours in movie). Concurrently, axons in nerve 4 make a sharp turn dorsally to innervate the fin via the ventral plexus. Thick axon bundles first grow perpendicular to muscle fibers near the proximal fin base, but subsequently axons turn posteriorly to grow mostly parallel to muscle fibers and towards the fin tip. As muscle fibers elongate, branching motor axons follow close behind to form a diffuse innervation network. At the end of the movie (after approximately 37 hours), a simplified innervation pattern is established. Frames are maximum projections through the developing pectoral fin at 30 minute increments. Stills from this timelapse were used in figure 2B. The movie plays at 4 frames per second. Scale bar is 25 microns.